T.R.
BOLU ABANT İZZET BAYSAL UNIVERSITY
INSTITUTE OF GRADUATE STUDIES
Department of Chemistry

FABRICATION of UNDOPED and (Mn, Ce, Eu, Tb) DOPED NICKEL BORATE NANOSIZED CERAMIC POWDERS

MASTER OF SCIENCE

UTKU YILDIRIM

ACADEMIC SUPERVISOR
Prof. Dr. AYŞE MORKAN
ACADEMIC CO-SUPERVISOR
Assoc. Prof. Dr. BAHADIR ALTINTAŞ

BOLU, JULY – 2024

APPROVAL OF THE THESIS

FABRICATION of UNDOPED and (Mn, Ce, Eu, Tb) DOPED NICKEL BORATE NANOSIZED CERAMIC POWDERS submitted by **UTKU YILDIRIM** and defended before the Examining Committe Members listed below in partial fulfillment of the requirements for the degree of **Master of Science** in **Department of Chemistry, Institute of Graduate Studies of Bolu Abant Izzet Baysal University in 29.07.2024** by

Examining Committee Members	**Signature**
Supervisor Prof. Dr. Ayşe MORKAN Bolu Abant Izzet Baysal University	.....
Member Prof. Dr. Fazilet Devrim ÖZDEMİRHAN Bolu Abant Izzet Baysal University	.....
Member Prof. Dr. Mecit AKSU Düzce University	.....

Prof. Dr. İbrahim KÜRTÜL

Director of Institute of Graduate Studies

ETHICAL DECLARATION

In this thesis dissertation that was properly prepared according to the Thesis Writing Rules of Bolu Abant İzzet Baysal University of the Institute of Graduates Studies, I hereby declare that;

- All data, information, and documents presented in the thesis were obtained in accordance with the academic and ethical rules,
- All data, documents, assessments, and results were presented in accordance with the scientific ethical and moral rules,
- All works that were benefitted in the thesis were appropriately cited,
- No alteration was made in the data used,
- Study presented in this thesis is original,

Otherwise, I declare that I accept the loss of all my rights in case any contradiction that may arise against me.

The similarity rate obtained by using the Turnitin program, a plagiarism detection software, is within the limits approved by the University Senate.

_____

UTKU YILDIRIM

ABSTRACT

FABRICATION of UNDOPED and (Mn, Ce, Eu, Tb) DOPED NICKEL BORATE NANOSIZED CERAMIC POWDERS
MSC THESIS
UTKU YILDIRIM
BOLU ABANT IZZET BAYSAL UNIVERSITY
INSTITUTE OF GRADUATE STUDIES
DEPARTMENT OF CHEMISTRY
(SUPERVISOR: PROF. DR. AYŞE MORKAN)
(CO-SUPERVISOR: ASSOC. PROF. DR. BAHADIR ALTINTAŞ)
BOLU, JULY 2024
(xii + 50)

In this work, the fabrication of undoped and doped nanosized nickel orthoborate ceramic powders was carried out by high temperature solid state synthesis method. The nickel orthoborates were prepared in two compositions with various dopant concentrations: manganese (II) doped, $Ni_3(BO_3)_2$: Mn^{2+} and 0.01 mol manganese (II) combined with rare earth metal, $Ni_3(BO_3)_2$: $0.01Mn^{2+}RE^{3+}$ (RE = Ce, Eu, and Tb).

All the synthesized materials were characterized using X-ray Diffraction (XRD), Infrared Spectroscopy (FTIR), Diffuse Reflectance Spectroscopy (DRS) and Thermogravimetric/Differential Thermal Analysis (TG/DTA) to determine their structural, chemical, optical and thermal properties, respectively.

XRD Data analysis indicated that highly crystalline $Ni_3(BO_3)_2$:Mn^{2+} has an optimal manganese concentration of 0.01 mol, with no changes in crystal structure upon doping. Additionally, FTIR techniques revealed that all the characteristic bands of orthoborates were observed between 2000–500 cm^{-1}.

DRS studies of $Ni_3(BO_3)_2$: $0.01Mn^{2+}xRE^{3+}$ revealed two dominant reflectance bands: at around 350-550 nm and 650-850 nm. Europium was found to be the most suitable co-activator, with an optimum concentration of 0.010 mol. Moreover, the reflectance bands shifted towards shorter wavelengths, moving from visible region to NIR-UV due to contributions from cerium, europium, and terbium.

Furthermore, the pure $Ni_3(BO_3)_2$ compound has a forbidden energy value of Eg = 3.148 eV. For $Ni_3(BO_3)_2$: Mn^{2+}, the values were found to range from 3.330-3.170 eV. In $Ni_3(BO_3)_2$: $0.010Mn^{2+}$ compounds doped with rare earth metals, the values ranged from 3.16-3.14 eV (cerium-doped), 3.32-3.36 eV (europium-doped), and 3.32-3.34 eV (terbium-doped). The TG/DTA analysis demonstrated an endothermic peak around 1380ºC for all samples.

KEYWORDS: XRD, FTIR, Nickel borate, TG/DTA, UV-VIS, DRS

ÖZET

KATKISIZ ve (Mn, Ce, Eu, Tb) KATKILI NİKEL BORAT NANOBOYUTLU SERAMİK TOZLARIN ÜRETİMİ
YÜKSEK LİSANS TEZİ
UTKU YILDIRIM
BOLU ABANT İZZET BAYSAL ÜNİVERSİTESİ
LİSANSÜSTÜ EĞİTİM ENSTİTÜSÜ
KIMYA ANABİLİM DALI
(TEZ DANIŞMANI: PROF. DR. AYŞE MORKAN)
(İKİNCİ DANIŞMAN: DOÇ. DR. BAHADIR ALTINTAŞ)
BOLU, TEMMUZ - 2024
(xii + 50)

Bu çalışmada katkısız ve katkılı nanoboyutlu nikel ortoborat seramik tozları, yüksek sıcaklık katı hal sentez yöntemiyle üretilmiştir. Nikel ortoboratlar, farklı katkı konsantrasyonlarında iki bileşimde hazırlanmıştır: mangan (II) katkılı, $Ni_3(BO_3)_2$: Mn^{2+} ve 0.01 mol mangan (II) ile nadir toprak metalinin birleşimi, $Ni_3(BO_3)_2$: $0.01Mn^{2+}RE^{3+}$ (RE = Ce, Eu ve Tb).

Sentezlenen tüm malzemelerin yapısal, kimyasal, optik ve termal özelliklerini belirlemek için X-Işını Difraksiyonu (XRD), Kızılötesi Spektroskopi (FTIR), Difüz Reflektans Spektroskopisi (DRS) ve Termogravimetrik/Diferansiyel Termal Analiz (TG/DTA) teknikleri ile karakterizasyonu yapılmıştır.

XRD veri analizi, yüksek kristalli $Ni_3(BO_3)_3$: Mn^{2+} bileşiğinin optimal mangan konsantrasyonunun 0.01 mol olduğunu ve katkı sonucunda kristal yapısında herhangi bir değişiklik olmadığını göstermektedir. Ayrıca, FTIR teknikleri, ortoboratlara ait tüm karakteristik bantların 2000–500 cm^{-1} arasında gözlemlendiğini ortaya koymuştur.

$Ni_3(BO_3)_2$: $0.01Mn^{2+}$+ RE^{3+} boratların DRS çalışmaları, yaklaşık 350-550 nm ve 650-850 nm aralığında iki baskın yansıma bandı ortaya koymuştur. Europyum, 0.010 mol optimum konsantrasyon ile en uygun ko-aktivator olarak bulunmuştur. Ayrıca, yansıma bantları, serium, europyum ve terbiyum katkıları nedeniyle görünür bölgeden NIR-UV'ye doğru daha kısa dalga boylarına kaymıştır.

Ayrıca, tek faz $Ni_3(BO_3)_2$ bileşiğinin yasak enerji değeri Eg = 3.148 eV'dir. $Ni_3(BO_3)_2$: Mn^{2+} bileşenleri için değerlerin 3.330-3.170 eV aralığında bulunduğu tespit edilmiştir.. $Ni_3(BO_3)_2$: $0.010Mn^{2+}$ ile nadir toprak metallerle katkılanmış bileşiklerde, değerler serium katkılı için 3.16-3.14 eV, europyum katkılı için 3.32-3.36 eV ve terbyum katkılı için 3.32-3.34 eV arasında değişmiştir. TG/DTA analizi, tüm örnekler için yaklaşık 1380ºC'de bir endotermik zirve göstermiştir.

ANAHTAR KELİMELER: XRD, FTIR, Nikel borat, TG/DTA, UV-VIS, DRS.

TABLE OF CONTENTS

Page

APPROVAL OF THE THESIS ..... **iii**

ETHICAL DECLARATION ..... **iv**

ABSTRACT ..... **v**

ÖZET ..... **vi**

TABLE OF CONTENTS ..... **vii**

LIST OF FIGURES ..... **ix**

LIST OF TABLES ..... **xi**

ACKNOWLEDGEMENT ..... **xii**

1. INTRODUCTION **1**

1.1 Literature Survey Related to Borates 2

2. AIM AND SCOPE OF THE STUDY **5**

3. MATERIALS AND METHODS **6**

3.1 CHEMICALS 6

3.2 INSTRUMENTS 6

3.2.1 Fourier Transform Infrared Spectrophotometer 6

3.2.2 X-ray Powder Diffractometer 6

3.2.3 UV- VIS Spectrometer 6

3.2.4 Furnace 7

3.3 SYNTHESIS METHODS 7

3.3.1 Synthesis of $Ni_3(BO_3)_2$ by Solid State Synthesis Method 7

4. RESULTS AND DISCUSSION **9**

4.1. XRD Characterization of $Ni_3(BO_3)_2$: Mn^{2+} and $Ni_3(BO_3)_2$: Mn^{2+}, RE^{3+} (RE= Ce, Eu, and Tb) 9

4.2. Infrared Spectra Characterization of the $Ni_3(BO_3)_2$: Mn^{2+} and $Ni_3(BO_3)_2$: Mn^{2+}, RE^{3+} (RE= Ce, Eu, Tb) 14

4.3. Thermogravimetric–Differential Thermal Analysis (TG/DTA) Data of $Ni_3(BO_3)_2$: Mn^{2+} and $Ni_3(BO_3)_2$: Mn^{2+}, RE^{3+} (RE= Ce, Eu, and Tb) 19

4.4. Study of Optical Properties by Diffuse Reflectance Spectroscopy ..21

4.4.1 Reflectance Spectra of $Ni_3(BO_3)_2$:Mn^{2+} and $Ni_3(BO_3)_2$:Mn^{2+}, RE^{3+} (RE= Ce, Eu, and Tb) 21

4.4.2 Calculation and Comparison of Forbidden Energy (Band Gap Energy) Intervals of $Ni_3(BO_3)_2$: Mn^{2+} Compounds 26

4.4.3 Calculation and Comparison of the Band Gap Energy Intervals of $Ni_3(BO_3)_2$: Mn^{2+}, RE^{3+} (RE = Ce, Eu, and Tb) Compounds 29

4.5. Jana2006 Analysis of Synthesized Materials and Calculation of Crystal Size, Density, Surface Area Using Debye-Scherrer Equation 36

4.5.1 Jana2006 Analysis of $Ni_3(BO_3)_2$: xMn^{2+} (0.00, 0.01, 0.05, 0.10) and Calculation of Crystal Size and Density, Surface Area Using Debye-Scherrer Equation 36

4.5.2 Jana 2006 Analysis $Ni_3(BO_3)_2$: of Mn^{2+} , RE^{3+} (RE = Ce, Eu, and Tb) Compounds and Calculation of Crystal Size, Density, Surface Area Using Debye-Scherrer Equation 38

5. CONCLUSIONS AND RECOMMENDATIONS 46

6. REFERENCES 49

LIST OF FIGURES

Page

Figure 4.1. The XRD patterns of $Ni_3(BO_3)_2$, $Ni_3(BO_3)_2$: xMn^{2+} (x= 0.01, 0.05, 0.10) 10
Figure 4.2. XRD patterns of $Ni_3(BO_3)_2$: $0.010Mn^{2+}$, xCe^{3+} (x= 0.000, 0.005, 0.010, 0.020) 11
Figure 4.3. XRD patterns of $Ni_3(BO_3)_2$: $0.010Mn^{2+}$, xEu^{3+} (x= 0.000, 0.005, 0.010, 0.020) 12
Figure 4.4. XRD patterns of $Ni_3(BO_3)_2$: $0.010Mn^{2+}$, xTb^{3+} (x= 0.000, 0.005, 0.010, 0.020) 13
Figure 4.5. Infrared spectra of $Ni_3(BO_3)_2$: $\mathbf{x}Mn^{2+}$, (**x**= 0.00, 0.01, 0.05, 0.10) 15
Figure 4.6. Infrared spectra of $Ni_3(BO_3)_2$: $0.010Mn^{2+}$, $\mathbf{x}Ce^{3+}$ (**x**= 0.000, 0.005, 0.010, 0.020)..... 16
Figure 4.7. Infrared spectra of $Ni_3(BO_3)_2$: $0.010Mn^{2+}$, $\mathbf{x}Eu^{3+}$ (**x**= 0.000, 0.005, 0.010, 0.020)..... 17
Figure 4.8. Infrared spectra of $Ni_3(BO_3)_2$: $0.010Mn^{2+}$, $\mathbf{x}Tb^{3+}$ (**x**= 0.000, 0.005, 0.010, 0.020)..... 18
Figure 4.9. Thermogravimetric – differential thermal analysis (TG/DTA) results of $Ni_3(BO_3)_2$, $Ni_3(BO_3)_2$: $0.010Mn^{2+}$ 19
Figure 4.10. Thermogravimetric – differential thermal analysis (TG/DTA) results of $Ni_3(BO_3)_2$: $0.010Mn^{2+}$, $\mathbf{x}Ce^{3+}$ (**x**= 0.005, 0.010, 0.020) 19
Figure 4.11. Thermogravimetric – differential thermal analysis (TG/DTA) results of $Ni_3(BO_3)_2$: $0.010Mn^{2+}$, $\mathbf{x}Eu^{3+}$ (**x**= 0.005, 0.010, 0.020) 20
Figure 4.12. Thermogravimetric – differential thermal analysis (TG/DTA) results of $Ni_3(BO_3)_2$: $0.010Mn^{2+}$, $\mathbf{x}Tb^{3+}$ (**x**= 0.005, 0.010, 0.020) 20
Figure 4.13. UV-Vis diffusive reflectance spectra of $Ni_3(BO_3)_2$: $\mathbf{x}Mn^{2+}$(**x**= 0.00, 0.01, 0.05, 0.10)..... 24
Figure 4.14. UV-Vis diffusive reflectance spectra of $Ni_3(BO_3)_2$: $0.010Mn^{2+}$, $\mathbf{x}Ce^{3+}$ (**x**= 0.000, 0.005, 0.010, 0.020) 24
Figure 4.15. UV-Vis diffusive reflectance spectra of $Ni_3(BO_3)_2$: $0.010Mn^{2+}$, $\mathbf{x}Eu^{3+}$ (**x**= 0.000, 0.005, 0.010, 0.020) 25
Figure 4.16. UV-Vis diffusive reflectance spectra of $Ni_3(BO_3)_2$: $0.010Mn^{2+}$, $\mathbf{x}Tb^{3+}$ (**x**= 0.000, 0.005, 0.010, 0.020) 25
Figure 4.17. Graph of change of $(\alpha h\nu)^2$ relative to hν for the calculation of the forbidden energy range of $Ni_3(BO_3)_2$ 27
Figure 4.18. Graph of change of $(\alpha h\nu)^2$ relative to hν for the calculation of the forbidden energy range $Ni_3(BO_3)_2$: $0.010Mn^{2+}$ 27
Figure 4.19. Graph of change of $(\alpha h\nu)^2$ relative to hν for the calculation of the forbidden energy range $Ni_3(BO_3)_2$: $0.050Mn^{2+}$ 28
Figure 4.20. Graph of change of $(\alpha h\nu)^2$ relative to hν for the calculation of the forbidden energy range $Ni_3(BO_3)_2$: $0.100Mn^{2+}$ 28
Figure 4.21. Graph of change of $(\alpha h\nu)^2$ relative to hν for the calculation of the forbidden energy range of $Ni_3(BO_3)_2$: $0.010Mn^{2+}$, $0.005Ce^{3+}$ 30
Figure 4.22. Graph of change of $(\alpha h\nu)^2$ relative to hν for the calculation of the forbidden energy range of $Ni_3(BO_3)_2$: $0.010Mn^{2+}$, $0.010Ce^{3+}$ 30
Figure 4.23. Graph of change of $(\alpha h\nu)^2$ relative to hν for the calculation of the forbidden energy range of $Ni_3(BO_3)_2$: $0.010Mn^{2+}$, $0.02Ce^{3+}$ 31

Figure 4.24. Comparison of forbidden energy ranges of $Ni_3(BO_3)_2$: $0.010Mn^{2+}$, **x**Ce^{3+} (**x**= 0.000, 0.005, 0.010, 0.020) compounds..... 31
Figure 4.25. Graph of change of $(\alpha h\nu)^2$ relative to $h\nu$ for the calculation of the forbidden energy range of $Ni_3(BO_3)_2$: $0.010Mn^{2+}$, $0.005Eu^{3+}$ 32
Figure 4.26. Graph of change of $(\alpha h\nu)^2$ relative to $h\nu$ for the calculation of the forbidden energy range of $Ni_3(BO_3)_2$: $0.010Mn^{2+}$, $0.010Eu^{3+}$ 32
Figure 4.27. Graph of change of $(\alpha h\nu)^2$ relative to $h\nu$ for the calculation of the forbidden energy range of $Ni_3(BO_3)_2$: $0.010Mn^{2+}$, $0.020Eu^{3+}$ 33
Figure 4.28. Comparison of forbidden energy ranges of $Ni_3(BO_3)_2$: $0.010Mn^{2+}$, **x**Eu^{3+} (**x**= 0.000, 0.005,0.010, 0.020) compounds 33
Figure 4.29. Graph of change of $(\alpha h\nu)^2$ relative to $h\nu$ for the calculation of the forbidden energy range of $Ni_3(BO_3)_2$: $0.010Mn^{2+}$, $0.005Tb^{3+}$ 34
Figure 4.30. Graph of change of $(\alpha h\nu)^2$ relative to $h\nu$ for the calculation of the forbidden energy range of $Ni_3(BO_3)_2$: $0.010Mn^{2+}$, $0.010Tb^{3+}$ 34
Figure 4.31. Graph of change of $(\alpha h\nu)^2$ relative to $h\nu$ for the calculation of the forbidden energy range of $Ni_3(BO_3)_2$: $0.010Mn^{2+}$, $0.020Tb^{3+}$ 35
Figure 4.32. Comparison of the forbidden energy ranges of $Ni_3(BO_3)_2$: $0.010Mn^{2+}$, xTb^{3+} (x = 0.000, 0.005, 0.010, 0.020) 35
Figure 4.33. Jana2006 analysis patterns for $Ni_3(BO_3)_2$: xMn^{2+} (0.00, 0.01, 0.05, 0.10) materials 36
Figure 4.34. Jana2006 analysis pattern of $Ni_3(BO_3)_2$: $0.010Mn^{2+}$, $0.005Ce^{3+}$ 38
Figure 4.35. Jana2006 analysis pattern of $Ni_3(BO_3)_2$: $0.010Mn^{2+}$, $0.010Ce^{3+}$ 39
Figure 4.36. Jana2006 analysis pattern of $Ni_3(BO_3)_2$: $0.010Mn^{2+}$, $0.020Ce^{3+}$ 39
Figure 4.37. Jana2006 analysis pattern of $Ni_3(BO_3)_2$: $0.010Mn^{2+}$, $0.005Eu^{3+}$ 40
Figure 4.38. Jana2006 analysis pattern of $Ni_3(BO_3)_2$: $0.010Mn^{2+}$, $0.010Eu^{3+}$ 40
Figure 4.39. Jana2006 analysis pattern of $Ni_3(BO_3)_2$: $0.010Mn^{2+}$, $0.020Eu^{3+}$ 41
Figure 4.40. Jana2006 analysis pattern of $Ni_3(BO_3)_2$: $0.010Mn^{2+}$, $0.005Tb^{3+}$ 41
Figure 4.41. Jana2006 analysis pattern of $Ni_3(BO_3)_2$: $0.010Mn^{2+}$, $0.010Tb^{3+}$ 42
Figure 4.42. Jana2006 analysis pattern of $Ni_3(BO_3)_2$: $0.010Mn^{2+}$, $0.020Tb^{3+}$ 42

LIST OF TABLES

Page

Table 4.1. Infrared vibration bands frequencies of the products obtained 14
Table 4.2. Percentage reflectance and absorbance values of the compounds in 350-550 nm range 22
Table 4.3. $Ni_3 (BO_3)_2$: xMn^{2+} (0.00, 0.01, 0.05, 0.10) Jana2006 detailed analysis results for the materials 37
Table 4.4. Detailed Jana2006 analysis results of $Ni_3(BO_3)_2$: $0.010Mn^{2+}$,xCe^{3+} (x= 0.000, 0.005, 0.010, 0.020) synthesized materials 43
Table 4.5. Detailed Jana2006 analysis results of $Ni_3(BO_3)_2$: $0.010Mn^{2+}$,xEu^{3+} (x= 0.000, 0.005, 0.010, 0.020) synthesized materials 44
Table 4.6. Detailed Jana2006 analysis results of $Ni_3(BO_3)_2$: $0.010Mn^{2+}$,xTb^{3+} (x= 0.000, 0.005, 0.010, 0.020) synthesized materials 45

ACKNOWLEDGEMENTS

I would like to express my deepest gratitude thanks to my supervisor, Prof. Dr. Ayşe MORKAN for her great guidance, honest advice, valuable criticism, continuous encouragements and insight throughout my master's studies. I has been a privilege to work under her supervision, and I am truly grateful for her contributions to my academic and professional growth.

I would like to express my sincere gratitude to my co-supervisor, Assoc. Dr. Bahadır ALTINTAŞ, for his invaluable support and guidance throughout my research journey. His expertise and insights were instrumental in shaping my understanding of the subject matter and enhancing the quality of my work.

I would also like to extend my heartfelt thanks to Dr. Esra Gül GÖĞCEGÖZ and Dr. Liska FADLIYANI for their assistance and support in the experimental work and in writing this thesis. Their collaboration and expertise greatly enriched my research experience, and I am grateful for their encouragement and dedication throughout this process.

I would also like to express my sincere gratitude to my family and my friends for their love, encouragement, and support during my thesis.

1. INTRODUCTION

In recent years, technological developments and their role in our daily life led the improvements of the available materials and synthesis of new functional materials. One of the most important improvements in the electronic technology is invention of transistor as a result of developments in the semiconductors physics.

The semiconductor device was developed in 1948 at Bell laboratories in ABD, by John Bardeen, Walter Houser Brittain and William Bradford Shockley. Transistors that can perform all the functions of electron lamps are devices which are much smaller and lighter, more resistant to mechanical effects, longer life, higher efficiency, less heat losses and much less power. With these characteristics, transistors have led to developments which can be described as revolution in the electronics industry [1].

The studies on semiconductors have been intensified and the use of semiconductor materials has been expanded together with transistors. Semiconductors are currently used as the basic material of the electronics industry in the production of many important devices including transistors, diodes, LEDs, gas sensors, processors, electroluminescence and photoluminescence devices, photodetectors and solar panels.

One of the criteria for the investigation of materials in terms of electrical conductivity is the energy band model. According to this model, the electrons in the last orbit of the atomic structure which gain energy are thought to jump to the empty band and provide conductivity. In the atomic and crystal structures of the metals, the energy band filled by electrons coincides with the empty energy band, so that the electrons in the filled band, which gain energy by forming an external electric field, can easily pass to the empty band and provide conductivity. In the insulator, the forbidden energy band between the two bands does not allow conductivity. The atomic structure of the material deteriorates until the electrons that provide the conductivity gain the energy to exceed this band.

Since the forbidden energy band in the semiconductor is narrow, conductivity can be achieved by exceeding the atomic and crystal structure intact, but excessive energies can damage the material. Semiconductors are also affected by the ambient temperature and gain the conductivity with small energy in hot

environments, while higher energy requirements are required for conductivity in cold environments.

Semiconductor materials are materials with a forbidden energy range of 1-4 eV. They are located between the conductor and the insulator. Because the forbidden energy gaps are large, electrons in the valence band cannot pass into the conductivity band without external influence (heat, light, etc.). When the electrons in the valence band gain enough energy, from heat, light or magnetic effect, to exceed the forbidden energy range, they pass through the conductivity band and provide the transmission.

UV-Vis diffuse reflectance (DRS) studies allow the optical properties of semiconductor powders to be examined. The results of the DRS studies can be used in Kubela Munk equation to calculate the optical forbidden energy range (Eg). In the Kubela Munk equation, F (R) is directly associated with the absorption constant (α) and the value of the absorption constant (α) is determined using the following equation;

$$F(R) \equiv \alpha = (1-R)^2 / 2R \qquad \text{(R: reflectance)}$$

The forbidden energy range (Eg) is calculated from the $(F(R)h\nu)^2$ versus hν graph. The energy value of the point where the linear part of this graph intersects the hν axis at $(\alpha h\nu)^2 = 0$ gives the forbidden energy value of the synthesized materials.

1.1 Literature Survey Related to Borates

Boron is an element commonly found on earth, rocks and water. The different properties of compounds made with various metal or nonmetallic elements allow the use of boron compounds in many industries [3]. Boron acts as non-metal in its compounds, but pure boron is an electrical conductor such as carbon. Borates are of great importance in the production of new nonlinear optical materials such as magnetic, catalytic, optical, fluorescence, phosphorescence and luminescence due to their unique crystal structure, highly polarized, excellent transparency and non-linear properties, good mechanical and chemical parameters [4-10]. Therefore, considering the properties of boron, it is understood that boron based materials are suitable for use in the production of semiconductor technology. The studies and research on use of boron is very important both in terms of technology and because of our country have 70% of boron reserves. Transition and rare earth metals have

great importance as additives to this type of material because of their structures and potential applications such as magnetics, optics. In addition, it is reported that significant improvements have been observed in the absorption properties of borates by the addition of these types of metals to borates and these compounds are used in making high-definition televisions plasma panels, electroluminescence instruments, fluorescent lamps, high pressure mercury lamps, UV lamps, fluoroscopic displays, condensed displays and storage panels [11-13].

Luminescence spectrum changes were examined when Eu^{2+} is added to $Ba_2Cd\ (BO_3)_2$ and luminescence peak was observed at 606 nm, stock shift was determined to be 11,000 cm1- [14].

The luminescence properties of the $Sr_2Mg(BO_3)_2$ compound were determined by UV excitation using Eu^{3+} and Eu^{2+} additives [15,16]. The photoluminescence properties of the phosphors prepared by Eu^{2+} doping of $BaZr\ (BO_3)_2$ and $SrAl_2B_2O_7$ by classical solid state method were investigated. Eu^{3+} ions in both compounds have been reported to emit a strong emission of 615 nm from the $^5D_0 \rightarrow {}^7F_2$ transition and so can be used in plasma imaging panels [17].

Luminescence activate lithium tetraborate, $Li_4B_2O_7$ was synthesized by Czochralski technique using Cu and Eu additives , and in the luminescence studies with Eu doped lithium tetraborate compound, blue emission peak at 370 nm in single crystal structure and red emission peak at 615 nm in glassy structure were determined. [18].

$Ca_3(BO_3)_2$ was synthesized by solid state reaction by adding Ce^{3+} ion at 0.00005 and 0.0001 ratios. Since undesired phases were observed in the high-concentration phosphorus, only the luminescence properties of the low-concentration were studied, and two emission peaks were reported at 392 and 420 nm [19].

The thermoluminescence properties of the compounds obtained by adding $Tm^{3+,}$ Tb^{3+} and Dy^{3+} to $Sr_2Mg(BO_3)_2$ compound prepared by high temperature solid state synthesis method were examined and emission bands of $Sr_2Mg(BO_3)_2$: 0.04 Dy compound were determined at 480, 579, 662, 755 nm [20].

The luminescence properties of another metal borate, $BaZr(BO_3)_2$: Eu, were investigated using vacuum UV and UV energies and reported that very different emission bands were observed at different excitation energies (VUV, UV) [21].

$Ba_{2(1-x)}Ce_xNa_xCa(BO_3)_2$ and $Ba_2Ca_{1-2x}Ce_xNa_x(BO_3)_2$ phosphors were obtained by high temperature solid state synthesis method and Na^+ ion was used as auxiliary activator here. The optimum concentrations were determined and the excitation and emission wavelengths of Ce^{3+} ion from two different lattice directions (Ba^{2+} and Ca^{2+} directions) were determined [22].

Tb^{3+} doped $NaSrBO_3$ phosphorus was synthesized by combustion method, thermoluminescence peak was observed at 161°C and it was reported that its intensity increased as the amount of doped ion increased. In addition, intense yellow emission band was observed at 544 nm when the photoluminescence property was examined under 236 nm UV light [23].

The present properties of these compounds for use in the above mentioned technologies are improved in a variety of ways. Sometimes morphological properties are changed by synthesis methods and sometimes they are applied to the required technological fields by adding different materials or metals with various properties. In this work, it was aimed to synthesize new compounds by adding cerium, europium and terbium rare earth metals together with manganese to nickel borate and to investigate the effects of these additives on the optical properties of these compounds.

2. AIM AND SCOPE OF THE STUDY

In this study, nanosized ceramic powders were synthesized by adding manganese (II) metal at a 0.01 molar concentration and rare earth metals such as cerium (III), europium (III), and terbium (III) at specific ratios to nickel borate. The effects of these additives on the optical properties of the nickel borate were investigated.

For this purpose, undoped nickel borate and doped with manganese and some rare earth metal nickel borate ceramic compounds were fabricated using the high-temperature solid-state synthesis method. The structural and optical properties of the resulting compounds were analyzed using various methods. These methods included X-ray diffraction (XRD), Infrared Spectroscopy (FTIR), Thermogravimetric/Differential Thermal Analysis (TG/DTA) and UV-Vis Diffuse Reflectance Spectroscopy (DRS). Additionally, crystal structure and surface area calculations were performed using Jana2006 software program.

The overall aim of this study is to understand the optical properties of rare earth metal-doped nickel borate compounds and to provide insights that could contribute to their potential application areas.

3. MATERIALS AND METHODS

3.1 CHEMICALS

The following chemicals were used in the synthesis of the products:

Nickel (II) nitrate hexahydrate, $Ni(NO_3)_2.6H_2O$: Merck, 99.00%

Manganese (II) sulfate monohydrate, $MnSO_4.H_2O$: Merck, 98.00%

Europium (III) nitrate pentahydrate, $Eu(NO_3)_3.5H_2O$: Fluka, 99.99%

Cerium (III) nitrate hexahydrate, $Ce(NO_3)_3.6H_2O$: Merck, 98.50%

Terbium (III) nitrate pentahydrate, $Tb(NO_3)_3.5H_2O$: Aldrich, 99.90%

Boric acid, H_3BO_3 : Fluka, 99.50%

Potassium Bromide, KBr (in spectroscopic grade) : Merck, 99.90%
It was used for making IR pellets. It was dried at 180°C about 2 hours before using

3.2 INSTRUMENTS

3.2.1 Fourier Transform Infrared Spectrophotometer

Infrared spectra of the final products were recorded by Shimadzu Fourier Transform Infrared (FTIR) spectrophotometer in the region of 4000-400 cm^{-1}. The spectra of the products were obtained by preparing the pellets that are consisted of 0.1500:0.0010 (wt/wt) of KBr:product ratio.

3.2.2 X-ray Powder Diffractometer

Rigaku miniflex and multiflex X-ray powder diffractometer were used to provide the structural properties of products using CuKα (30-40 kV, 10-20mA, λ=1.54056 Å) radiation. The data of each XRD pattern were obtained by using Rigaku programs and checked by using ICDD data card.

3.2.3 UV- VIS Spectrometer

Perkin Elmer Lambda 35 UV-VIS Spectroscopy was used to determine the optical properties of the samples. The spectra were recorded at wavelength range of 200-900nm. The data was plotted by using Data Processor WinLab.

3.2.4 Furnace

The reactions during the preparation of metal borates were carried out at heating range between 400-900°C by the aid of Nuve MF 120 furnace.

3.3 SYNTHESIS METHODS

3.3.1 Synthesis of $Ni_3(BO_3)_2$ by Solid State Synthesis Method

Nickel (II) borate ($Ni_3(BO_3)_2$) was synthesized using nickel (II) nitrate hexahydrate ($Ni(NO_3)_2 \cdot 6H_2O$) and boric acid (H_3BO_3), as starting materials through the conventional high temperature solid state synthesis method. $Ni(NO_3)_2 \cdot 6H_2O$ and H_3BO_3 were used as the nickel and boron sources, respectively, with a Ni : B molar ratio of 3:2.

Stoichiometric amount of nickel (II) nitrate hexahydrate ($Ni(NO_3)_2 \cdot 6H_2O$) and boric acid (H_3BO_3), were mixed and grinded together in an agate mortar. A homogenized mixture was transfered into a convenient porcelain crucible and placed into the furnace. The main products were obtained in four steps;

Firstly, the temperature was raised up to 450^oC with an increase of 15^oC per minute. After being held for 4 hours at 450^oC, the mixture was taken out from the oven and cooled down and placed to the oven back again after crushing and blending well.

Secondly, the temperature was raised up to 600^oC with an increase of 1^oC per min and the mixture was held for 3 hours at 600^oC. In the third stage, the specimen was heated four times to 900^oC with an increase of 1^oC per min and was held for 12 hours.

Finally, the product was cooled down to the room temperature with a decrease of 1^oC per min.

At the end of each heating period, the mixtures were weighed, ground well and subjected to X-ray and IR analysis. A small amount of the precursor gel was set aside for further thermal analysis. The crystal structure and phase purity of the synthesized $Ni_3(BO_3)_2$ were examined by X-Ray Diffraction (XRD). The chemical bonds were analyzed using Fourier Transform Infrared (FTIR) Spectroscopy, and the optical properties were evaluated by UV-Vis Diffuse Reflectance Spectroscopy. The theoretical reaction for the preparation of undoped $Ni_3(BO_3)_2$ is considered as follows;

- **Solid State Reaction of Undoped $Ni_3(BO_3)_2$**

$$Ni(NO_3)_2{\cdot}6H_2O(s) + H_3BO(s) \rightarrow Ni_3(BO_3)_{2(s)} + 3N_{2(g)} + 6H_2O_{(g)} + NO_{2(g)}$$

- **Solid State Reactions of $(3\text{-}x)Ni(NO_3)_2.6H_2O + xMnSO_4.H_2O + 2H_3BO_3$**

The amounts of starting materials calculated with the molar ratios changing x values, $Ni(NO_3)_2.6H_2O : MnSO_4.H_2O : H_3BO_3 = 3\text{-}x : x : 2$ (x=0, 0.01, 0.05, 0.10). Taken stoichiometric amounts of these powders were weighted separately and homogeneously mixed in an agate mortar with a pestle. Each homogenized mixtures was transffered into a convenient porcelain crucible and placed into the furnace. The main products were obtained with four periods explained in previous section. The following reactions are predicted:

For x= 0,

$$3Ni(NO_3)_2.6H_2O_{(s)} + 2H_3BO_{3(s)} \rightarrow Ni_3(BO_3)_{2(s)} + 6NO_{2(g)} + 21H_2O_{(g)} + 1.5O_{2(g)}$$

For x= 0.01,

$$2.99Ni(NO_3)_2.6H_2O_{(s)} + 0.01MnSO_4.H_2O_{(s)} + 2H_3BO_{3(s)} \rightarrow Ni_{2.99}Mn_{0.01}(BO_3)_{2(s)} + 5.98NO_{2(g)} + 0.01SO_{2(g)} + 20.95H_2O_{(g)} + 1.5O_{2(g)}$$

For x= 0.05,

$$2.95Ni(NO_3)_2.6H_2O_{(s)} + 0.05MnSO_4.H_2O_{(s)} + 2H_3BO_{3(s)} \rightarrow Ni_{2.95}Mn_{0.05}(BO_3)_{2(s)} + 5.9NO_{2(g)} + 0.05SO_{2(g)} + 20.75H_2O_{(g)} + 1.5O_{2(g)}$$

For x= 0.10,

$$2.90Ni(NO_3)_2.6H_2O_{(s)} + 0.1MnSO_4.H_2O_{(s)} + 2H_3BO_{3(s)} \rightarrow Ni_{2.90}Mn_{0.10}(BO_3)_{2(s)} + 5.8NO_{2(g)} + 0.1SO_{2(g)} + 20.5H_2O_{(g)} + 1.5O_{2(g)}$$

Manganase and rare earth element doped nickel borates given by the formula $Ni_3(BO_3)_2$: $0.01Mn^{2+}$ xRE^{3+} (RE = Ce^{3+}, Eu^{3+}, Tb^{3+}, x = 0.000, 0.005, 0.010, 0.020) $Ni_3RE_x(BO_3)_2$ (RE= Ce^{3+}, Eu^{3+}, Tb^{3+}) were also synthesized by using the similar procedures with various concentrations of each rare earth element (x=0.005, 0.010, 0.020).

4. RESULTS AND DISCUSSION

4.1. XRD Characterization of $Ni_3(BO_3)_2$: Mn^{2+} and $Ni_3(BO_3)_2$: Mn^{2+}, RE^{3+} (RE= Ce, Eu, and Tb)

In the first stage of this study, it was planned to synthesize nickel orthoborates with manganese (II) and cerium (III), europium (III), terbium (III) doped by conventional high temperature solid state method. In order to make this synthesis, $Ni(NO_3)_2.6H_2O$ (Merck), $MnSO_4.H_2O$ (Merck), $Ce(NO_3)_3.6H_2O$ (Merck), $Eu(NO_3)_3.5H_2O$ (Fluka) and $Tb(NO_3)_3.5H_2O$ (Aldrich), H_3BO_3 (Fluka) were used. The substances were weighed separately in stoichiometric proportions; agate mortar was mixed homogeneously and crushed. Then, the mixtures were synthesized by heating in high temperature furnace at 450ºC for 4 hours, 600ºC for 3 hours, and 900ºC for 48 hours. At the end of each heating, the materials were cooled to room temperature, homogeneously mixed and crushed. Characterization of the resulting products was carried out using X-ray powder diffraction and infrared spectroscopic techniques.

First, the pure nickel borate and only manganese doped nickel borate were obtained from the solid state reaction and the XRD patterns of the products obtained are given in Figure 4.1. When XRD pattern of synthesized nickel borate was compared with ICDD 75-1809, it was observed that single phase nickel borate compound was obtained. Then, the optimum concentration value in moles for manganese (II) in manganese (II) doped nickel borate synthesis by the same method with at 0.01, 0.05 and 0.10 moles was determined as 0.010 mole, in other words, when the manganese (II) metal was added at 0.010 mole the nickel phase did not cause any change in the crystal structure.

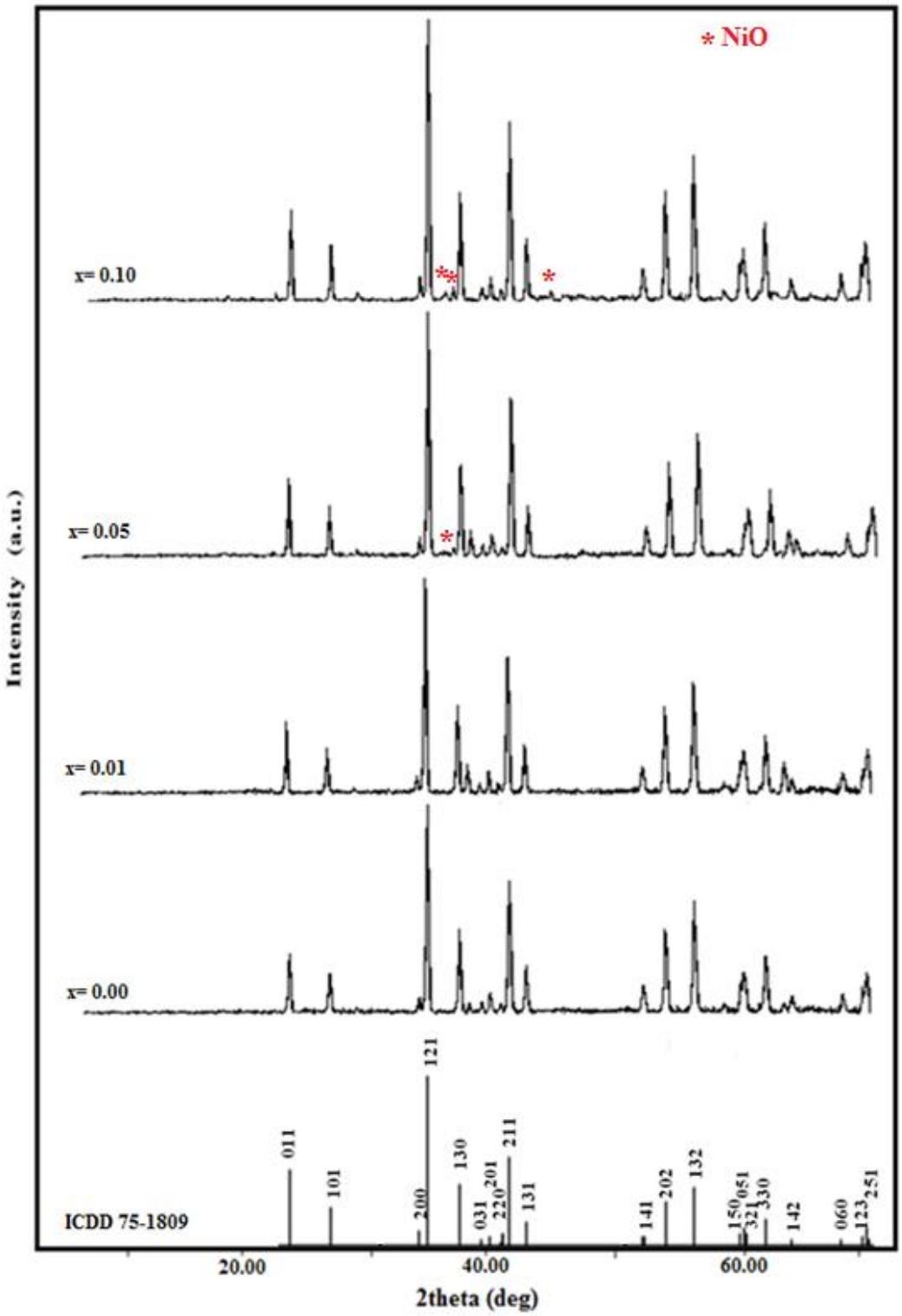

Figure 4.1. The XRD patterns of $Ni_3(BO_3)_2$, $Ni_3(BO_3)_2$: xMn^{2+} (x= 0.01, 0.05, 0.10)

In the continuation of the study, cerium (III), europium (III), terbium (III) rare earth metals were added separately with manganese (II) contribution. The XRD patterns of the products obtained are shown in Figure 4.2, Figure 4.3 and Figure

4.4, respectively. $Ni_3(BO_3)_2$: $0.010Mn^{2+}$, Ce^{3+} was added to the moles of 0.010 moles of manganese together with 0.005, 0.010, 0.020 moles of cerium oxide nickel borate. It is clear that the product obtained by adding cerium oxide in the ratio of 0.005 moles has the same diffraction peaks of the pure nickel borate compound with the XRD pattern given in Figure 4.2 and all belong to the nickel borate compound (ICDD no: 75–1809). Very little diffraction peaks of cerium oxide were observed in XRD patterns of the compounds added with 0.010 and 0.020 ratio of Ce^{3+} (Figure 4.2).

In the XRD patterns of nickel borate compounds doped with manganese (II) at a ratio of 0.010 moles to europium (III), terbium (III) with 0.005, 0.010, 0.020 moles, the diffraction peaks all belong to the nickel borate compound only (ICDD 75-1809).

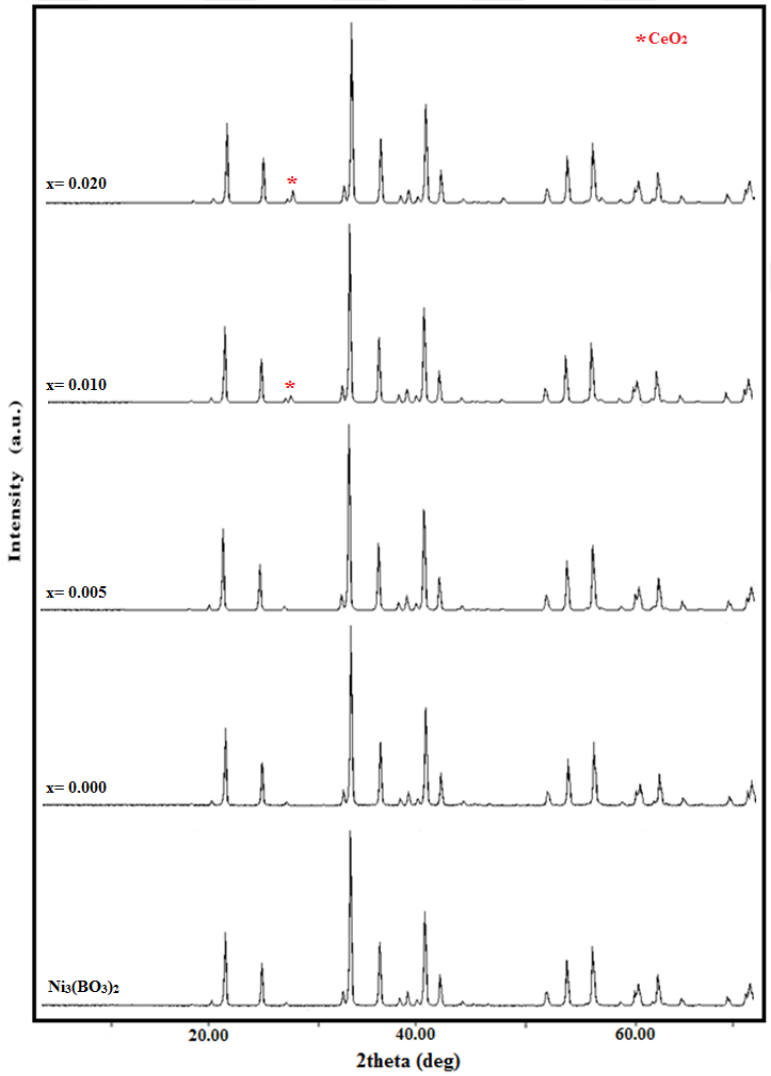

Figure 4.2. XRD patterns of $Ni_3(BO_3)_2$: $0.010Mn^{2+}$, xCe^{3+} (x= 0.000, 0.005, 0.010, 0.020)

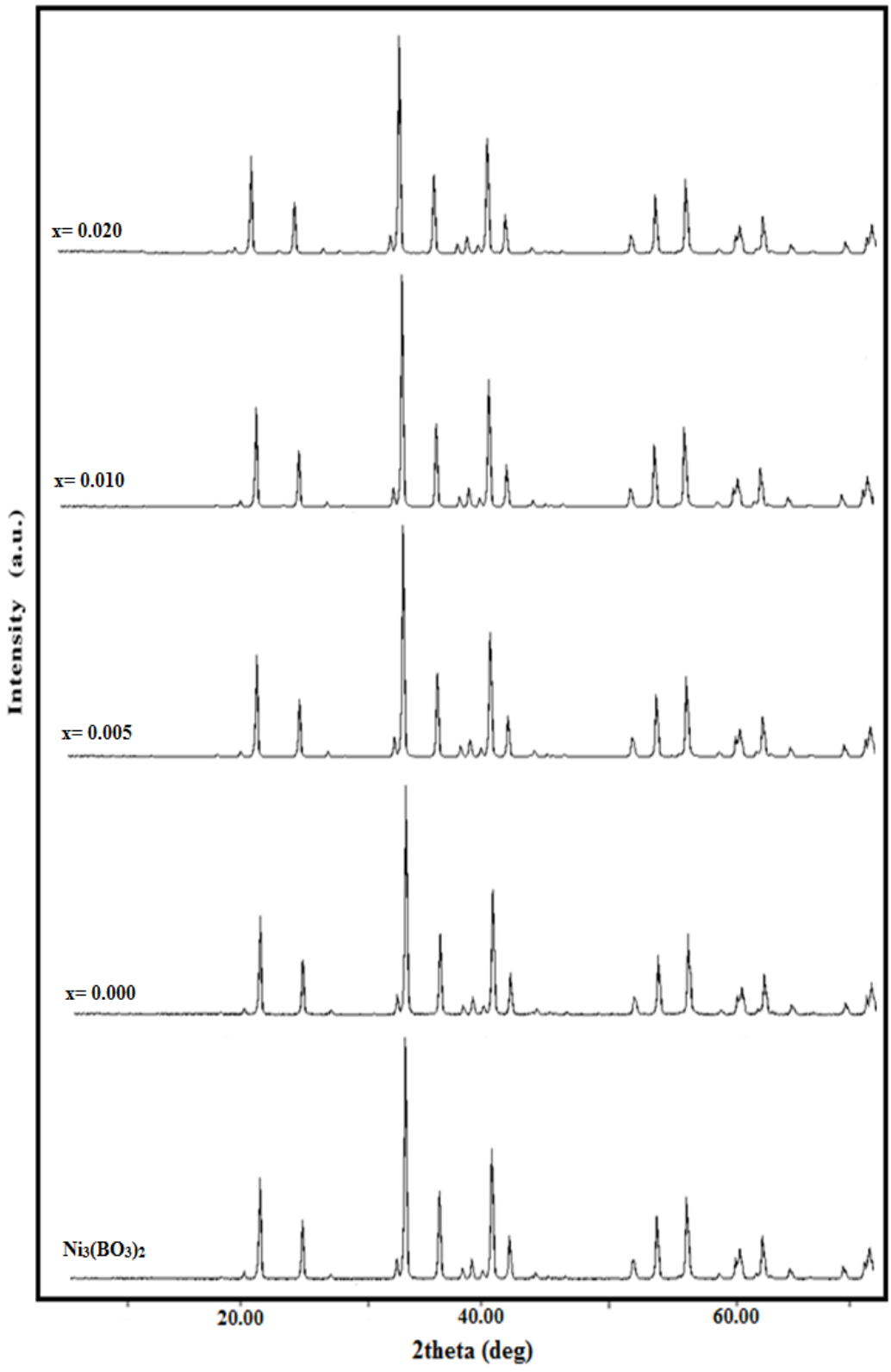

Figure 4.3. XRD patterns of $Ni_3(BO_3)_2$: $0.010Mn^{2+}$, xEu^{3+} (x= 0.000, 0.005, 0.010, 0.020)

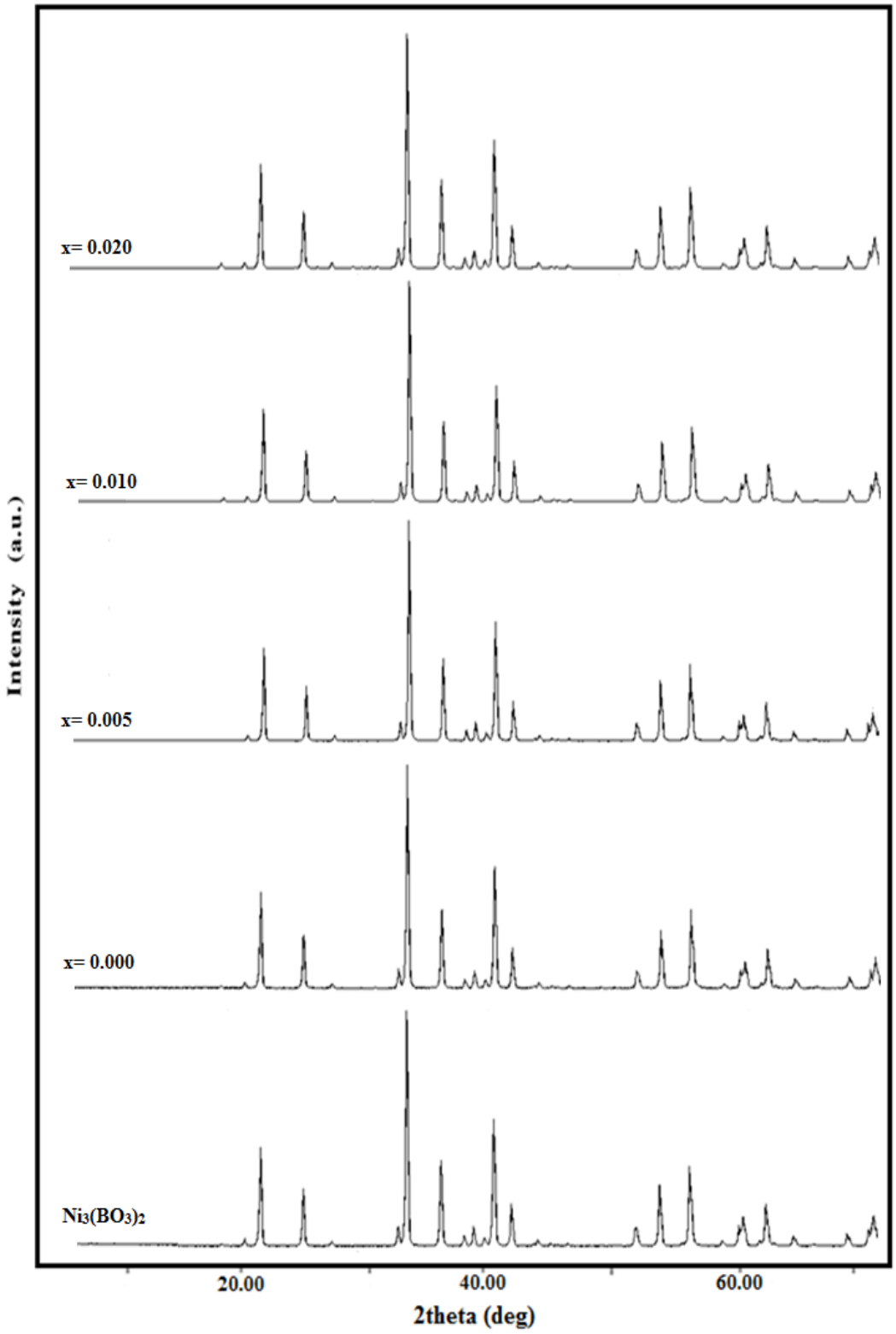

Figure 4.4. XRD patterns of $Ni_3(BO_3)_2$: $0.010Mn^{2+}$, xTb^{3+} (x= 0.000, 0.005, 0.010, 0.020)

4.2. Infrared Spectra Characterization of the $Ni_3(BO_3)_2$: Mn^{2+} and $Ni_3(BO_3)_2$: Mn^{2+}, RE^{3+} (RE= Ce, Eu, Tb)

The infrared spectra of the products obtained are given in Figure 4.5, Figure 4.6 and Figure 4.7. When infrared spectra are examined, it is seen that there are vibration bands of nickel borate compound parallel to XRD patterns. In the infrared spectra of borates, the vibration bands are concentrated in the range of 2000–500 cm^{-1} and the vibration modes of the borates are in three regions. The first region is in the range of 1200-1600 cm^{-1}, where there are vibration bands resulting from asymmetric stretching relaxation in the B-O bond in the BO_3 unit. The second zone is in the range of 800-1200 cm^{-1}, where the vibration bands are stressed by B-O bonds in the tetrahedron BO_4 unit. The last zone is about 700 cm^{-1}, where the vibration bands are due to B-O-B bonds in the crystal [24-28]. Based on this information, infrared results appear to be parallel to XRD patterns. The frequencies of the infrared vibration bands are given in Table 4.1.

Table 4.1. Infrared vibration band frequencies of the products obtained

Assignment	$\nu_2(BO_3)$	$\nu_1(BO_3)$	$\nu_3(BO_3)$	νOH
$Ni_3(BO_3)_2$	514	721, 632	1294, 1261, 1188	3412
$Ni_3(BO_3)_2$: 0.010Mn^{2+}	514	717, 627	1292, 1257, 1188	-
$Ni_3(BO_3)_2$: 0.010Mn^{2+},0.005 Ce^{3+}	513	717, 628	1291, 1261, 1184	3429
$Ni_3(BO_3)_2$: 0.010Mn^{2+}, 0.010Ce^{3+}	513	715, 628	1284, 1257, 1186	-
$Ni_3(BO_3)_2$: 0.010Mn^{2+},0.020 Ce^{3+}	515	717, 628	1288, 1262, 1186	3452
$Ni_3(BO_3)_2$: 0.010Mn^{2+},0.005 Eu^{3+}	514	719, 627	1288, 1263, 1184	-
$Ni_3(BO_3)_2$: 0.010Mn^{2+}, 0.010Eu^{3+}	513	715, 628	1287, 1255, 1180	-
$Ni_3(BO_3)_2$: 0.010Mn^{2+}, 0.020 Eu^{3+}	515	717, 630	1292,1260, 1186	-
$Ni_3(BO_3)_2$: 0.010Mn^{2+}, 0.005 Tb^{3+}	517	719, 629	1288, 1263, 1184	-
$Ni_3(BO_3)_2$: 0.010Mn^{2+}, 0.010Tb^{3+}	509	715, 628	1286, 1260, 1184	-
$Ni_3(BO_3)_2$: 0.010Mn^{2+}, 0.020 Tb^{3+}	518	715, 628	1286, 1257, 1182	3450

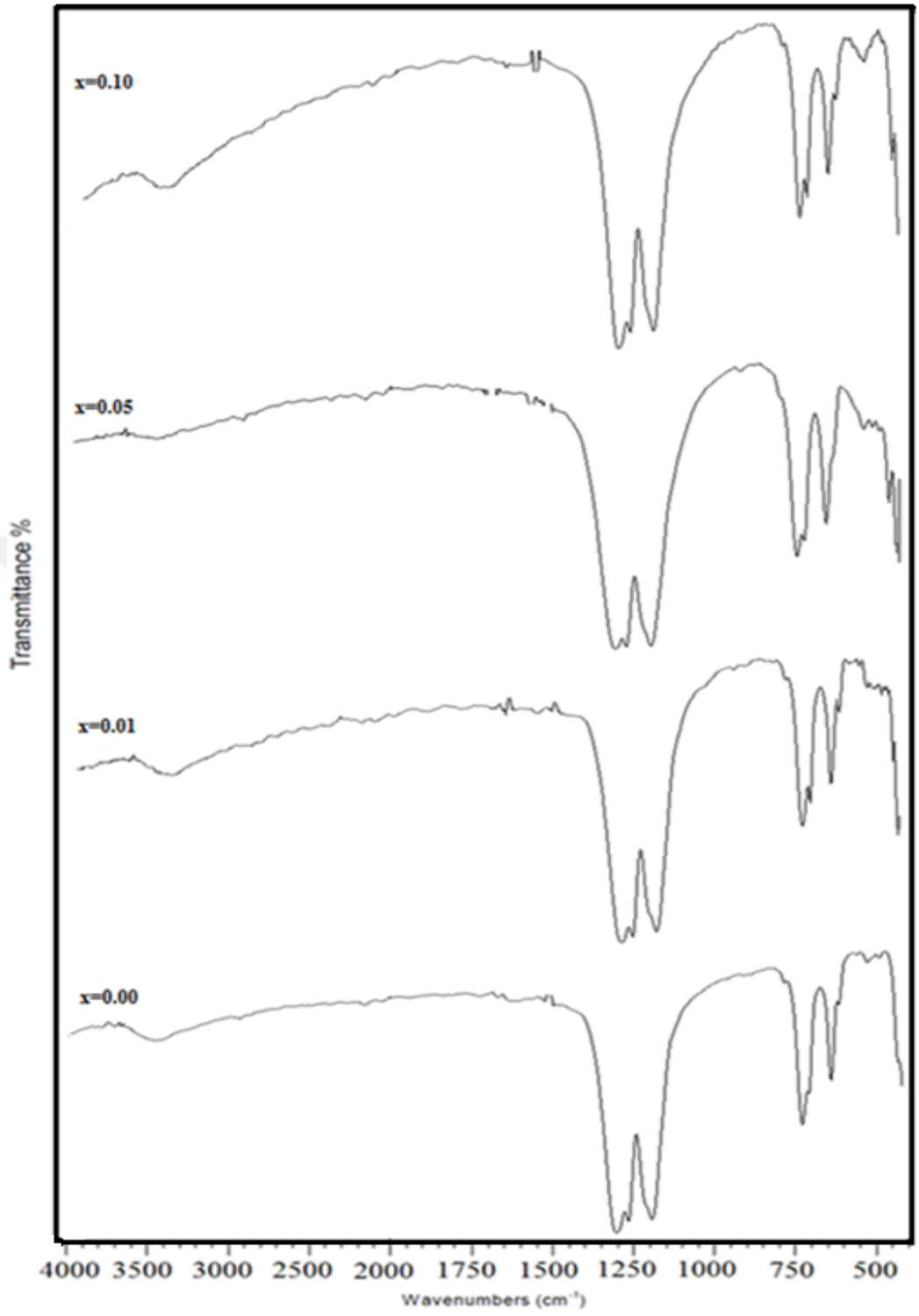

Figure 4.5. Infrared spectra of $Ni_3(BO_3)_2$: **x**Mn^{2+}, (**x**= 0.00, 0.01, 0.05, 0.10)

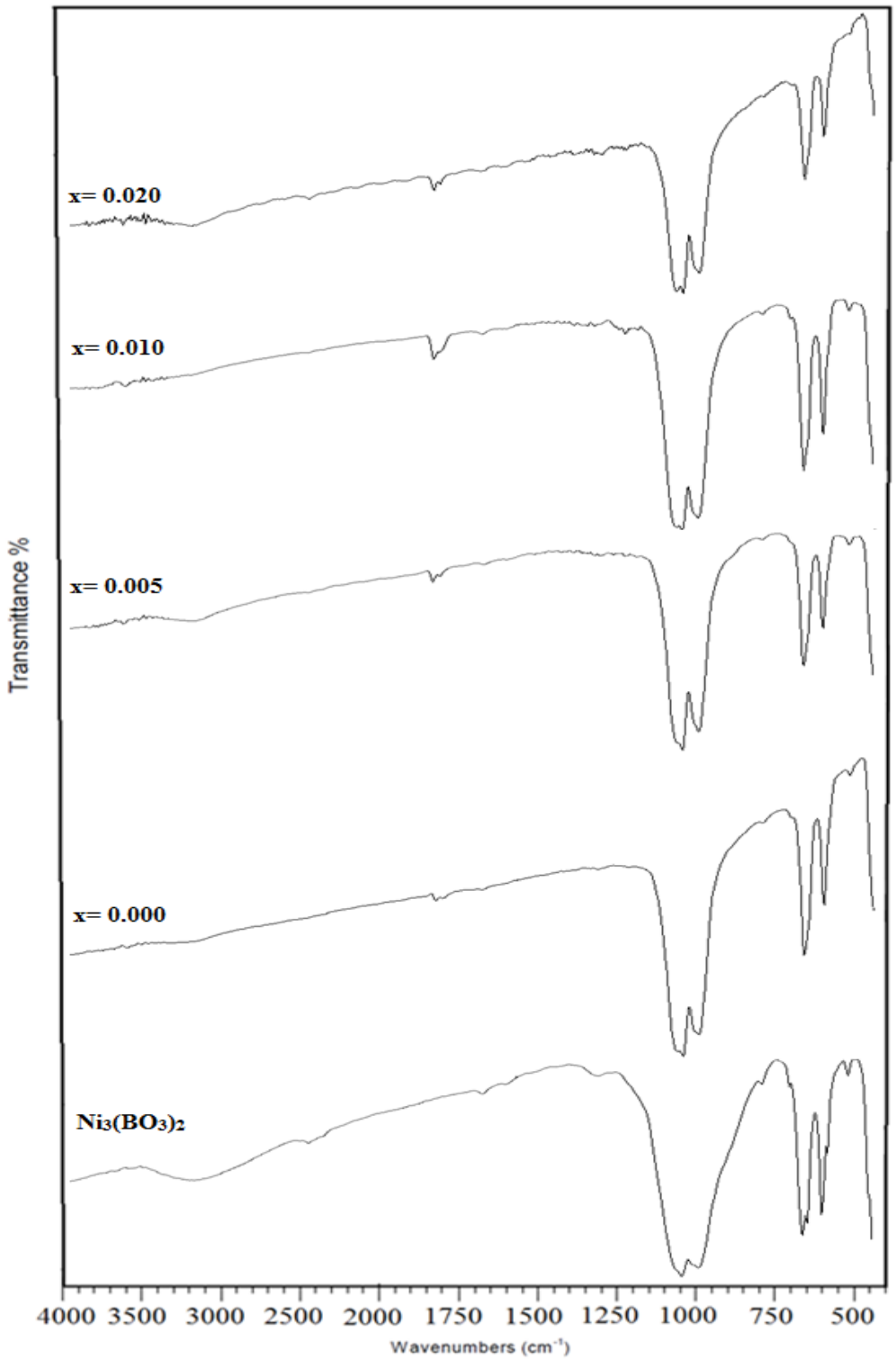

Figure 4.6. Infrared spectra of $Ni_3(BO_3)_2$: $0.010Mn^{2+}$, $\mathbf{x}Ce^{3+}$ (**x**= 0.000, 0.005, 0.010, 0.020)

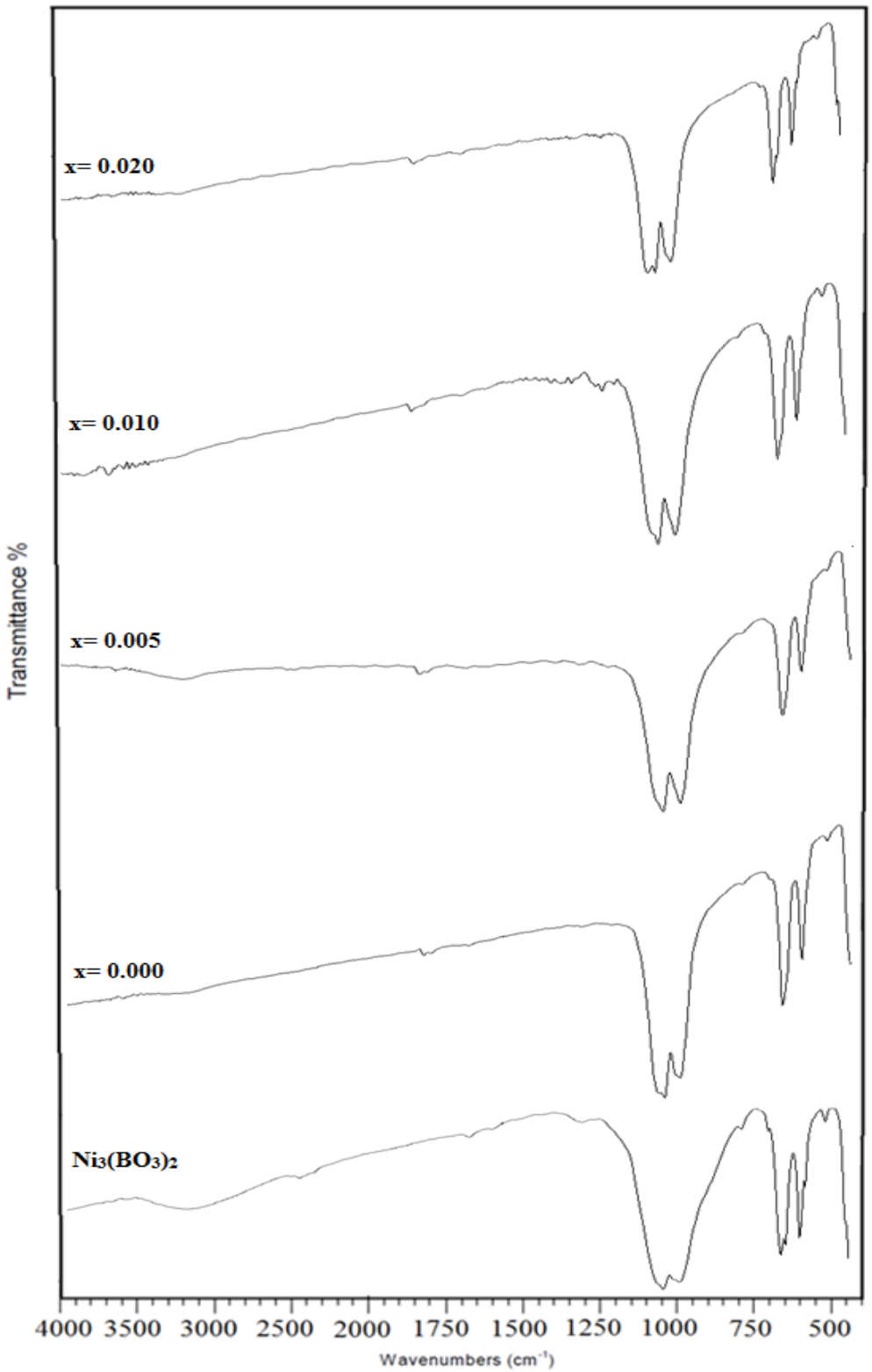

Figure 4.7. Infrared spectra of $Ni_3(BO_3)_2$: 0.010Mn^{2+}, **x**Eu^{3+} (**x**= 0.000, 0.005, 0.010, 0.020)

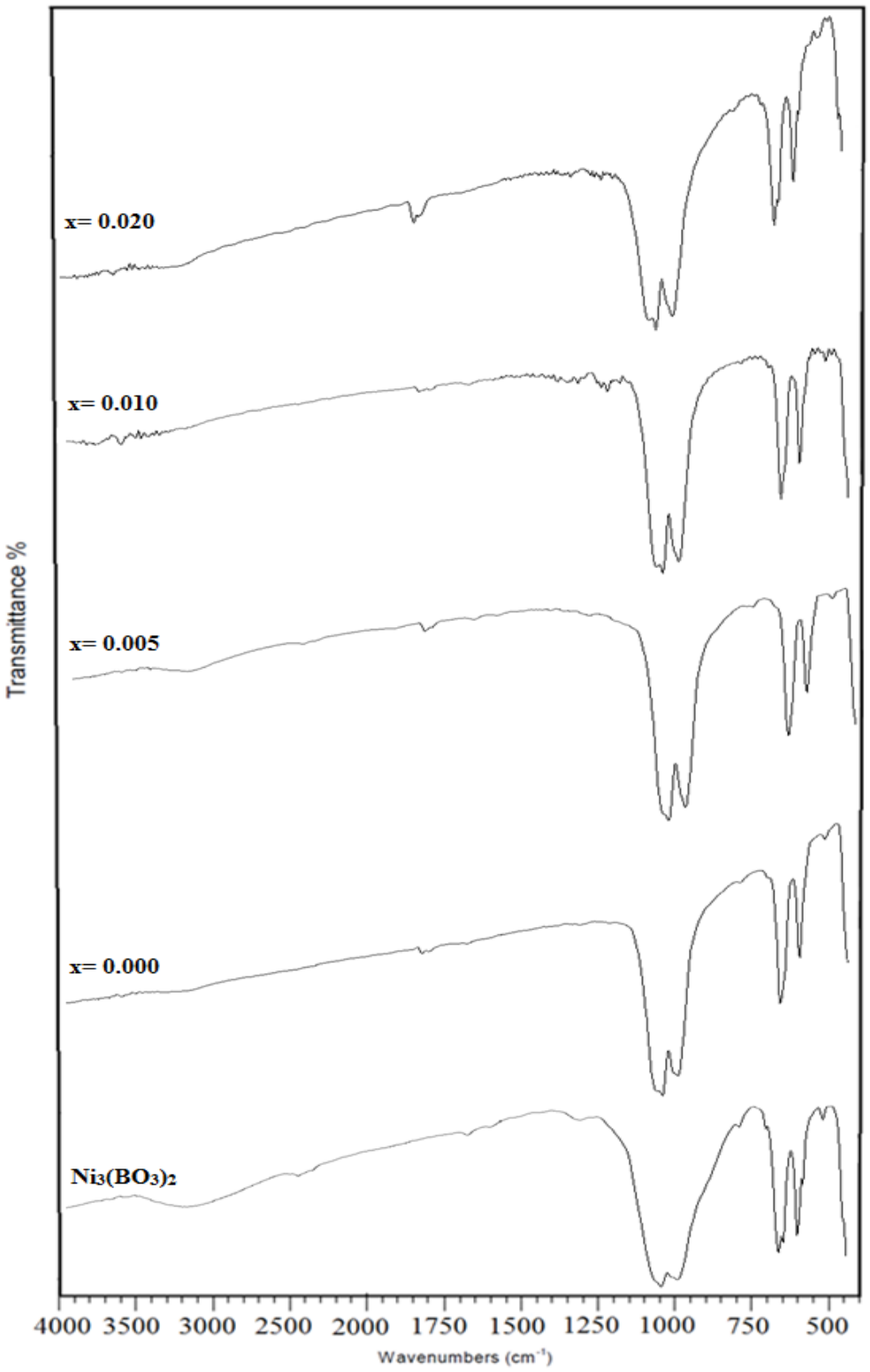

Figure 4.8. Infrared spectra of $Ni_3(BO_3)_2$: $0.010Mn^{2+}$, $\mathbf{x}Tb^{3+}$ (**x**= 0.000, 0.005, 0.010, 0.020)

4.3. Thermogravimetric–Differential Thermal Analysis (TG/DTA) Data of $Ni_3(BO_3)_2$: Mn^{2+} and $Ni_3(BO_3)_2$: Mn^{2+}, RE^{3+} (RE= Ce, Eu, and Tb)

When the thermogravimetric analysis-differential thermal analysis (TG/DTA) data given in Figure 4.9 are examined, it is seen that there is only endothermic peak around 1380ºC. This observed endothermic peak is thought to be the melting point of the nickel borate compound.

Figures 4.10, 4.11 and 4.12 show the results of thermogravimetric analysis-differential thermal analysis (TG/DTA) of nickel borate compounds with manganese (II) and cerium (III), europium (III), terbium (III), respectively. As a result, it is clear that there is no significant change in the value of the endothermic peak, which is considered to be the melting point when rare earth metals are added, since the amounts added are very small.

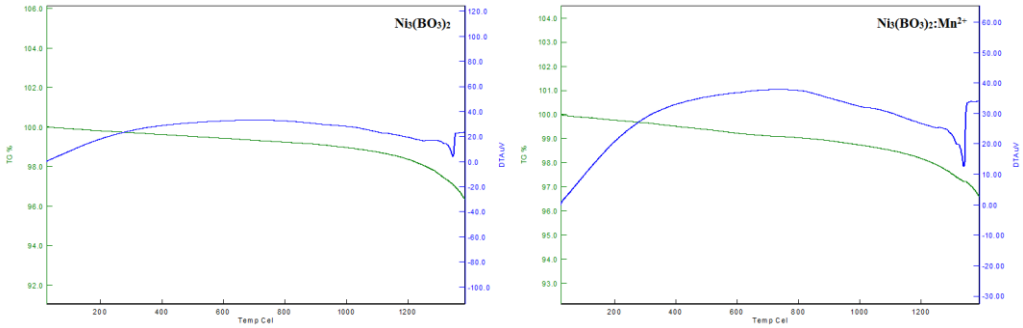

Figure 4.9. Thermogravimetric – differential thermal analysis (TG/DTA) results of $Ni_3(BO_3)_2$, $Ni_3(BO_3)_2$: $0.010Mn^{2+}$

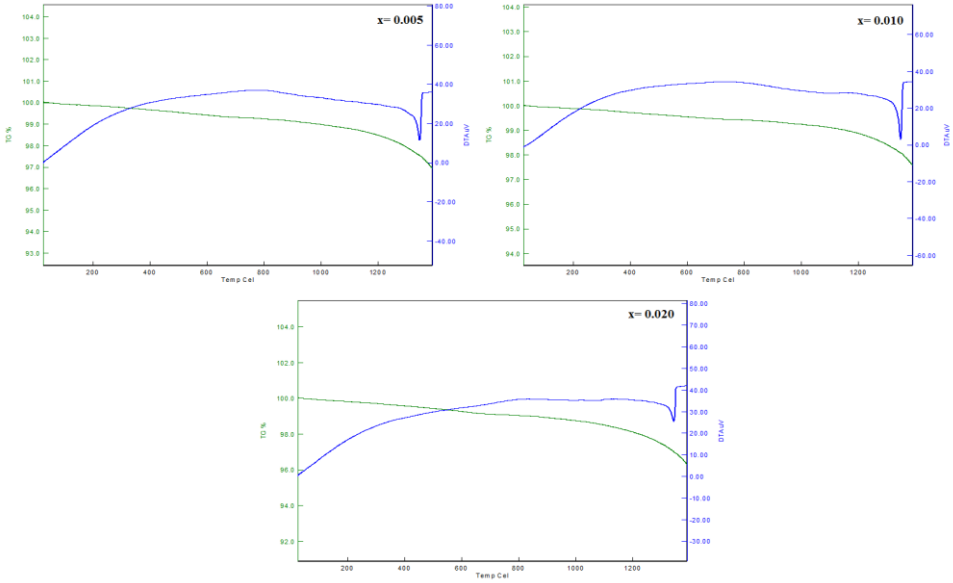

Figure 4.10. Thermogravimetric – differential thermal analysis (TG/DTA) results of $Ni_3(BO_3)_2$: $0.010Mn^{2+}$, $\mathbf{x}Ce^{3+}$ (**x**= 0.005, 0.010, 0.020)

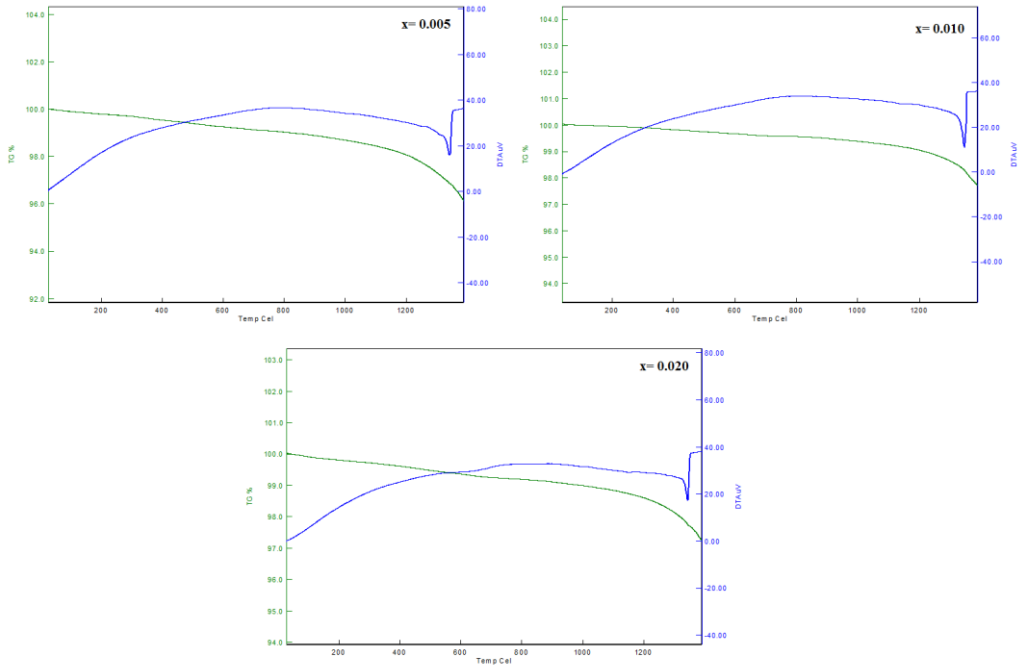

Figure 4.11. Thermogravimetric – differential thermal analysis (TG/DTA) results of $Ni_3(BO_3)_2$: $0.010Mn^{2+}$, $\mathbf{x}Eu^{3+}$ (**x**= 0.005, 0.010, 0.020)

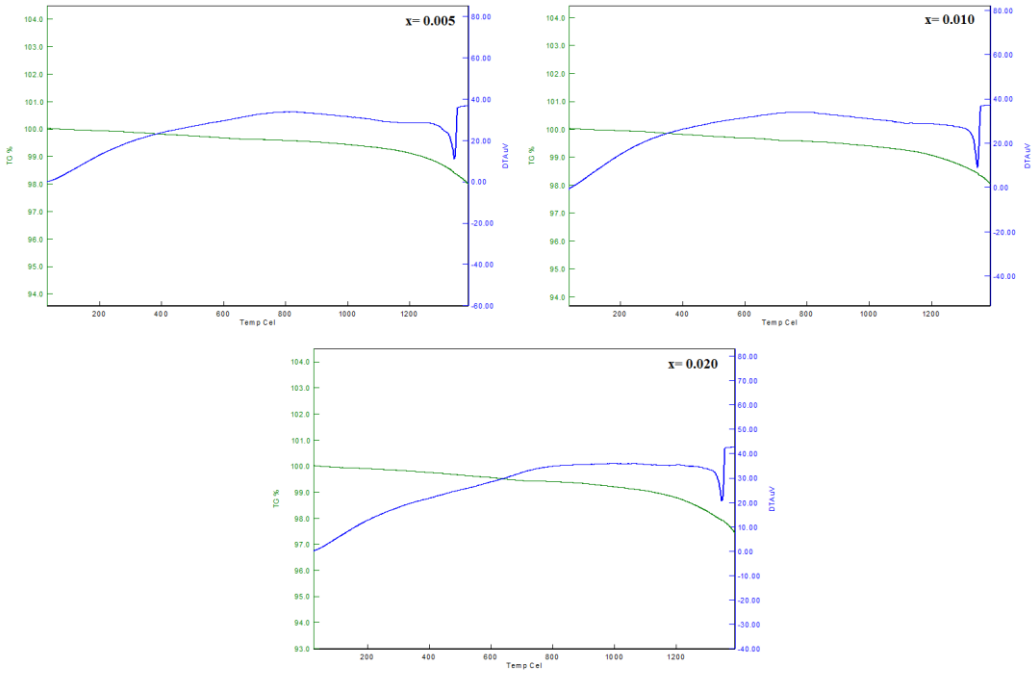

Figure 4.12. Thermogravimetric – differential thermal analysis (TG/DTA) results of $Ni_3(BO_3)_2$: $0.010Mn^{2+}$, $\mathbf{x}Tb^{3+}$ (**x**= 0.005, 0.010, 0.020)

4.4. Study of Optical Properties by Diffuse Reflectance Spectroscopy

4.4.1. Reflectance Spectra of $Ni_3(BO_3)_2:Mn^{2+}$ and $Ni_3(BO_3)_2:Mn^{2+}$, RE^{3+} (RE= Ce, Eu, and Tb)

In the second part of this study, diffuse reflectance studies of Mn^{2+}, RE^{3+} (RE = Ce, Eu, and Tb) doped nickel orthoborate, $Ni_3(BO_3)_2$ compounds synthesized in the first stage of the project using manganese (II) and cerium (Ce), europium (Eu) and terbium (Tb) metals by high temperature solid state method at 900 ºC were performed.

As it is known, many transition-metal ions absorb in the UV or visible region of the spectrum. For lanthanide and actinide series metals, the process takes place by electronic transitions of 4f and 5f electrons; for the first and second series of transition-metals, 3d and 4d electrons are responsible for the absorption.

For this reason, three types of electronic transitions are observed in the optical absorption spectra of synthesized compounds: charge transfer, d-d intra atomic (transition metal origin) and f-f intra atomic (originating from lanthanide ions) electron transitions.

The diffuse reflectance spectra made with synthesized doped $Ni_3(BO_3)_2$: Mn^{2+}, RE^{3+} (RE = Ce, Eu, and Tb) compounds are given in Figure 4.13, Figure 4.14, Figure 4.15 and Figure 4.16, respectively. In order to investigate the effects of auxiliary activators in the structure of nickel orthoborate compound on diffuse reflectance, the amount of rare earth metals added was changed.

In Figure 4.14, $Ni_3(BO_3)_2$: $0.010Mn^{2+}$, xCe^{3+} (x = 0.000, 0.005, 0.010, 0.020), when the reflectance spectra of the compounds were examined, the reflectance value of the pure nickel borate compound is the highest and approximately %2 decreases in reflectance value were observed with manganese additive. It was observed that the reflectance value decreased by 1% when 0.005 cerium was added as an auxiliary activator with manganese. Then, when the amount of cerium was continued to increase, it was observed that the reflectance value started to increase. However, when compared with pure nickel borate compound, it is seen that the reflectance values of cerium doped compounds are low. This shows us that our compound will have a higher radiation value than the pure state with the additives made in the 350-550 nm range, the highest absorption value of $Ni_3(BO_3)_2$: $0.010Mn^{2+}$, $0.005Ce^{3+}$ compound (4% more relative to the pure $Ni_3(BO_3)_2$).

Figure 4.15 shows the reflectance spectra of $Ni_3(BO_3)_2$: $0.010Mn^{2+}$, xEu^{3+} (x = 0.000, 0.005, 0.010, 0.020) compounds doped with europium auxiliary activator. When the spectra were examined, it was found that the reflectance value of pure nickel borate compound was highest as in cerium doped compounds. It was determined that the reflectance value decreases as the amount of europium additive increases and reaches the minimum value at x = 0.010 and increases again at x = 0.020. From this result, it is concluded that $Ni_3(BO_3)_2$: $0.010Mn^{2+}$, $0.010\ Eu^{3+}$ absorbs ~ 5% more light than $Ni_3(BO_3)_2$: $0.010Mn^{2+}$ and ~ 8% more light than pure $Ni_3(BO_3)_2$ in the range of 350-550 nm.

The diffuse reflectance spectra of $Ni_3(BO_3)_2$: $0.010Mn^{2+}$, Tb^{3+} (x = 0.000, 0.005, 0.010, 0.020) compounds with terbium co-activator are given in Figure 4.16. Only with the manganese addition, there is a certain decrease in reflectance, i.e. a certain increase in absorption. When terbium is added to this compound, it is seen that the reflectance value decreases further and increases with increasing the amount of terbium. $Ni_3(BO_3)_2$: $0.010Mn^{2+}$, $0.005Tb^{3+}$ compound has the lowest reflectance value, i.e. the highest absorption value (~ 5% higher than pure $Ni_3(BO_3)_2$ compound). Detailed percent reflectance and absorbance values of the compounds are given in Table 4.2.

In general, when UV-Vis diffuse reflectance properties are examined, it is seen that all of the compounds have two dominant wide reflectance bands which are in the range of 350-550 nm and 650-850 nm. Furthermore, it was observed that the reflectance bands shifted to low wavelengths from visible region wavelengths to NIR-UV wavelengths with the contribution of cerium, europium and terbium. It has been observed that the absorption value increases when only manganese is added to our pure nickel borate compound, but this value increases more when the auxiliary activator is used. In this study, the effects of the type and amount of the auxiliary activator on the absorbance were determined using UV-diffuse reflectance. It has been found that the most suitable co-activator for the nickel borate compound is europium among the rare earth metals used and the optimum concentration value is 0.010.

Table 4.2. Percentage reflectance and absorbance values of the compounds in 350-550 nm range

Name	R%	A%
$Ni_3(BO_3)_2$	16,915	83,085
$Ni_3(BO_3)_2$: **0.010**Mn^{2+}	14,436	85,564
$Ni_3(BO_3)_2$: **0.050**Mn^{2+}	14,126	85,874
$Ni_3(BO_3)_2$: **0.100**Mn^{2+}	8,136	91,864
$Ni_3(BO_3)_2$: **0.010**Mn^{2+},**0.005**Ce^{3+}	13,176	86,824
$Ni_3(BO_3)_2$: **0.010**Mn^{2+},**0.010**Ce^{3}	14,226	85,774
$Ni_3(BO_3)_2$: **0.010**Mn^{2+},**0.020**Ce^{3}	15,182	84,818
$Ni_3(BO_3)_2$: **0.010**Mn^{2+},**0.005**Eu^{3+}	10,296	89,704
$Ni_3(BO_3)_2$: **0.010**Mn^{2+},**0.010** Eu^{3+}	09,822	90,178
$Ni_3(BO_3)_2$: **0.010**Mn^{2+},**0.020** Eu^{3+}	11,634	88,366
$Ni_3(BO_3)_2$: **0.010**Mn^{2+},**0.005**Tb^{3+}	12,050	87,950
$Ni_3(BO_3)_2$: **0.010**Mn^{2+},**0.010** Tb^{3+}	12,301	87,699
$Ni_3(BO_3)_2$: **0.010**Mn^{2+},**0.020** Tb^{3+}	14,451	85,549

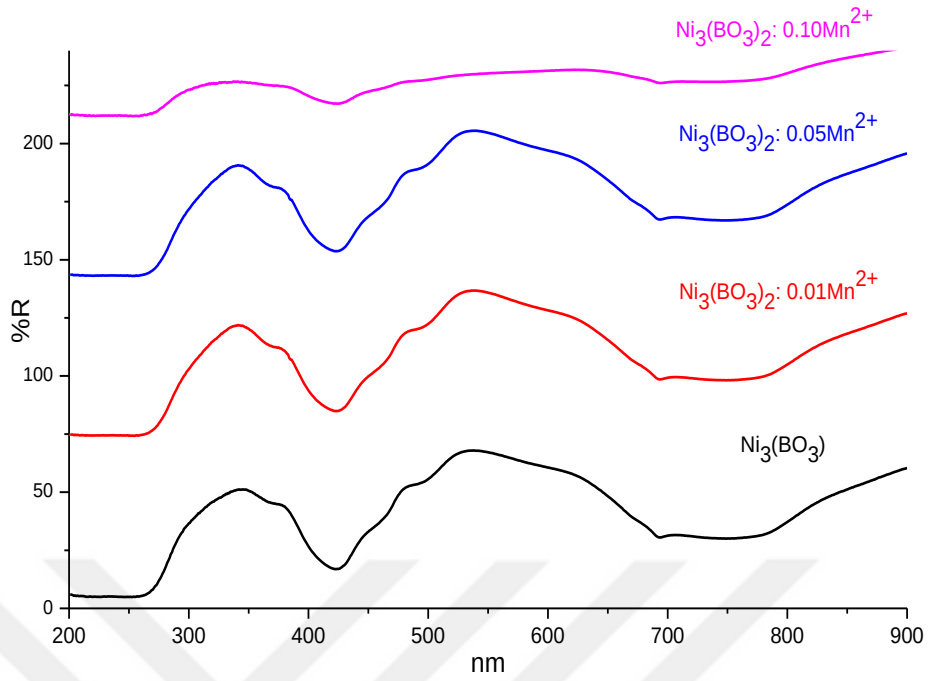

Figure 4.13. UV-Vis diffusive reflectance spectra of $Ni_3(BO_3)_2$: **x**Mn^{2+}(**x**= 0.00, 0.01, 0.05, 0.10)

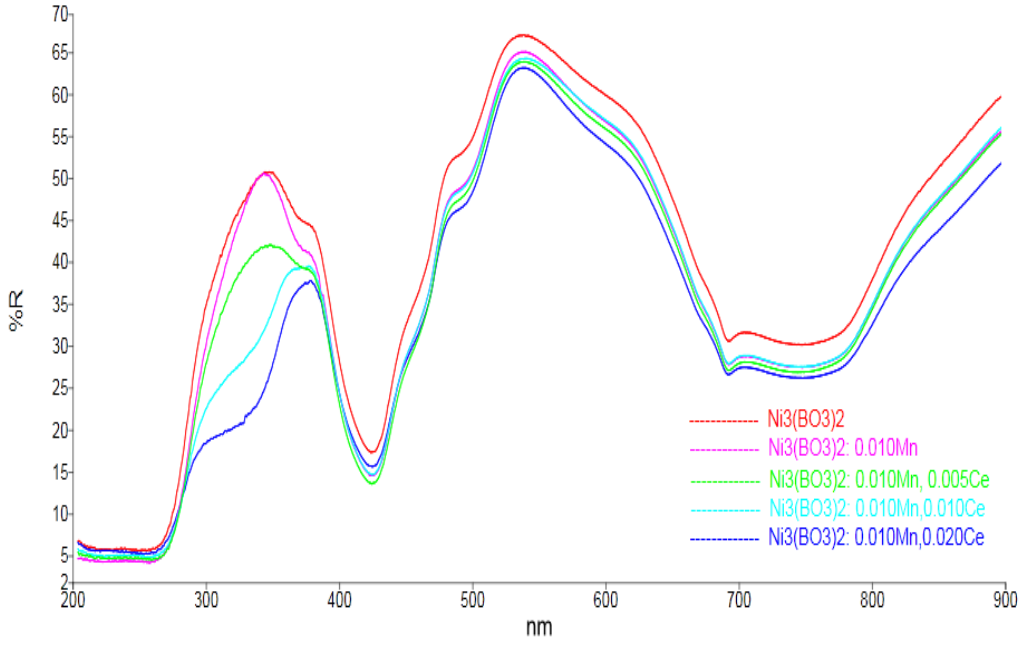

Figure 4.14. UV-Vis diffusive reflectance spectra of $Ni_3(BO_3)_2$: 0.010Mn^{2+}, **x**Ce^{3+} (**x**= 0.000, 0.005, 0.010, 0.020)

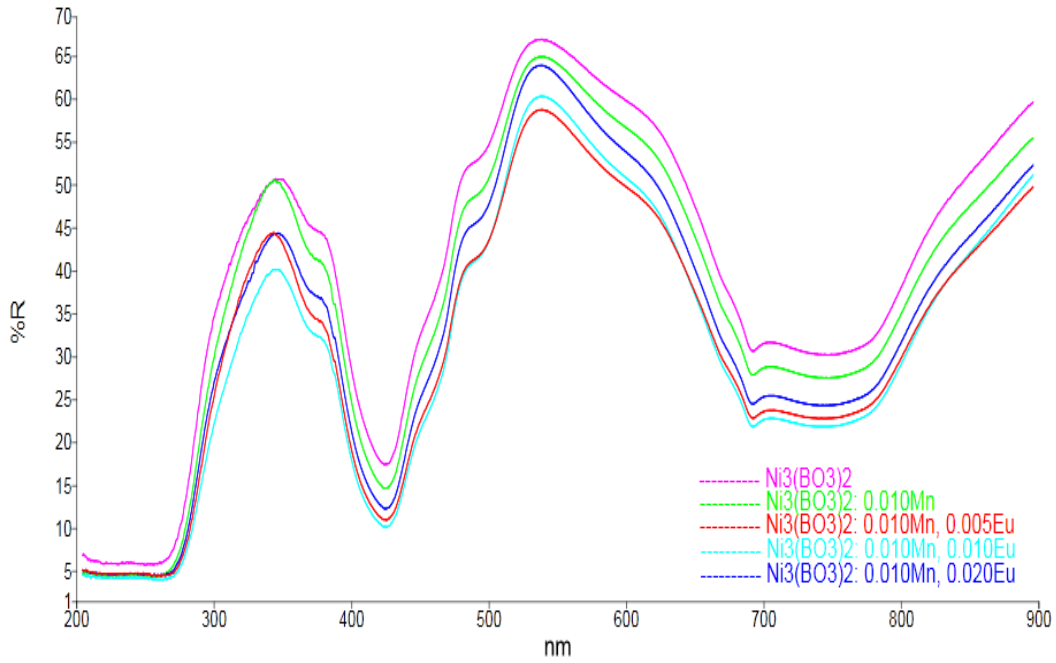

Figure 4.15. UV-Vis diffusive reflectance spectra of $Ni_3(BO_3)_2$: $0.010Mn^{2+}$, **x**Eu^{3+} (**x**= 0.000, 0.005, 0.010, 0.020)

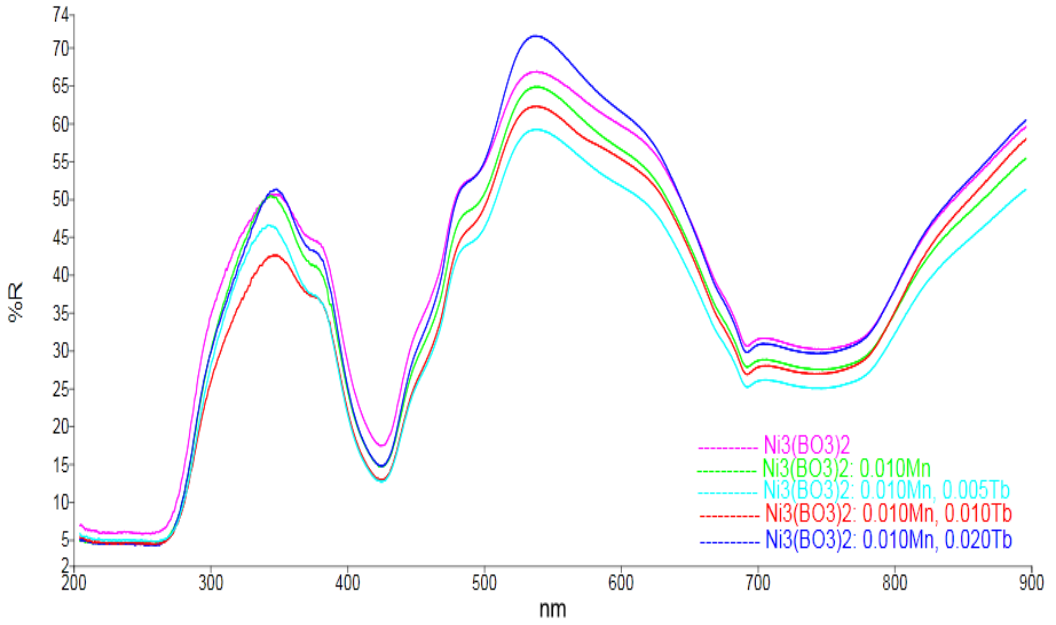

Figure 4.16. UV-Vis diffusive reflectance spectra of $Ni_3(BO_3)_2$: $0.010Mn^{2+}$, **x**Tb^{3+} (**x**= 0.000, 0.005, 0.010, 0.020)

4.4.2. Calculation and Comparison of Forbidden Energy (Band Gap Energy) Intervals of $Ni_3(BO_3)_2$: Mn^{2+} Compounds

In order to determine the forbidden energy ranges of the doped materials obtained, the $(\alpha h\nu)^2$ versus $h\nu$ change graphs of each material were drawn. The energy value of the point at which the linear part of these graphs intersect the $h\nu$ axis at $(\alpha h\nu)^2 = 0$ gives the forbidden energy value of the synthesized materials. Figure 4.17 shows the variation of $(\alpha h\nu)^2$ obtained by the absorption spectrum obtained at room temperature of the pure $Ni_3(BO_3)_2$ compound according to the photon energy. This forbidden energy value was found to be Eg = 3.148 eV.

Change graphs of $(\alpha h\nu)^2$ versus $h\nu$ for 0.010, 0.050 and 0.100 molar concentrations of manganese (II) doped $Ni_3(BO_3)_2$ compounds are plotted and given in Figure 4.17, Figure 4.18 and Figure 4.19, respectively. The point at which the linear parts of the graphs in the figures intersect the $h\nu$ axis gives the forbidden energy range. These forbidden energy ranges of 0.010, 0.050 and 0.100 molar manganese (II) doped compounds were found to be Eg = 3.330 eV, Eg = 3.216 eV and Eg = 3.170 eV, respectively. The comparison of the forbidden energy ranges of $Ni_3(BO_3)_2$: xMn^{2+} (x: 0, 0.01, 0.05 and 0.10) is given in graphical form or better understanding of the change of forbidden energy ranges with the amount of manganese in $Ni_3(BO_3)_2$ compound.

It has been found that as the amount of manganese in the material increases, the forbidden energy range starts to increase, as the amount of manganese continues to increase, the forbidden energy range starts to decrease. These results show that the optimum concentration of manganese (II) is 0.01 molar for the addition of other rare earth metals.

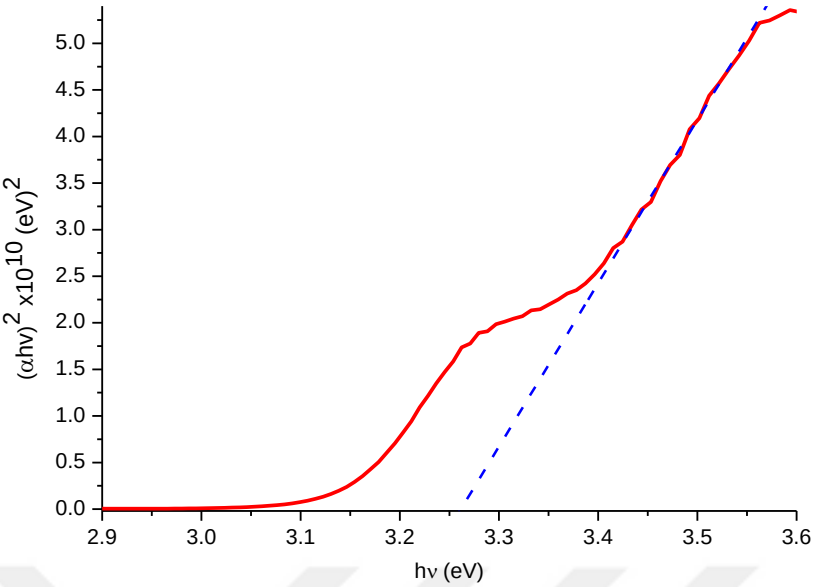

Figure 4.17. Graph of change of $(\alpha h\nu)^2$ relative to hν for the calculation of the forbidden energy range of $Ni_3(BO_3)_2$

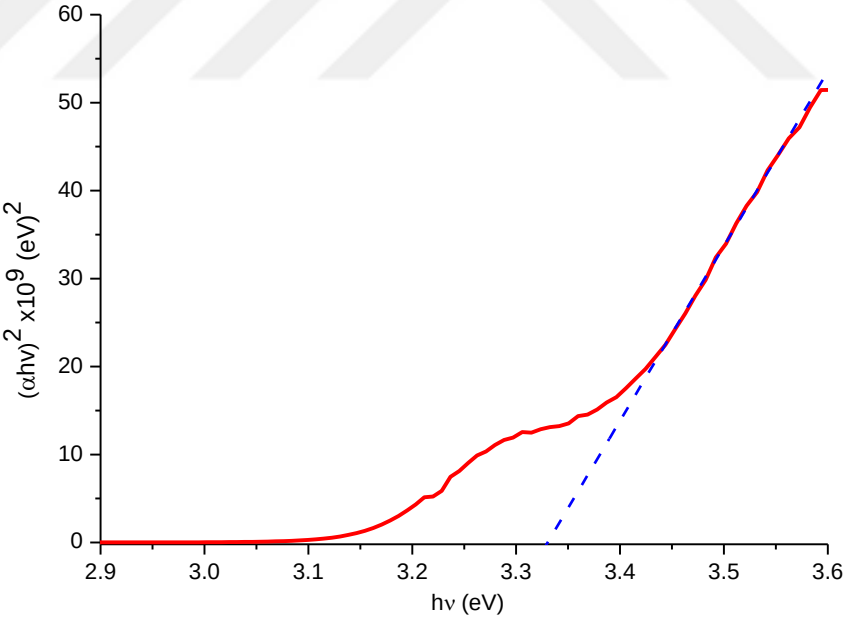

Figure 4.18. Graph of change of $(\alpha h\nu)^2$ relative to hν for the calculation of the forbidden energy range $Ni_3(BO_3)_2$: $0.010Mn^{2+}$

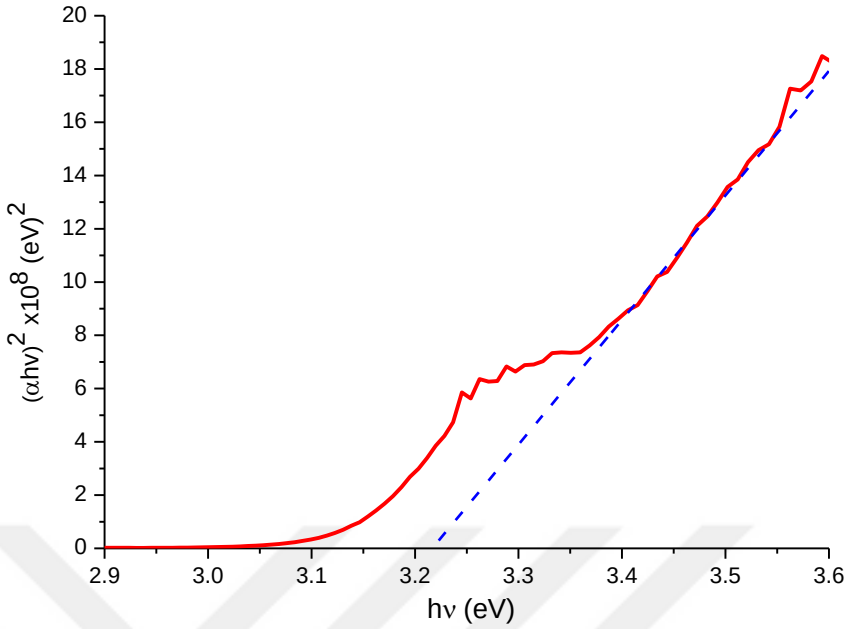

Figure 4.19. Graph of change of $(\alpha h\nu)^2$ relative to hν for the calculation of the forbidden energy range $Ni_3(BO_3)_2$: $0.050Mn^{2+}$

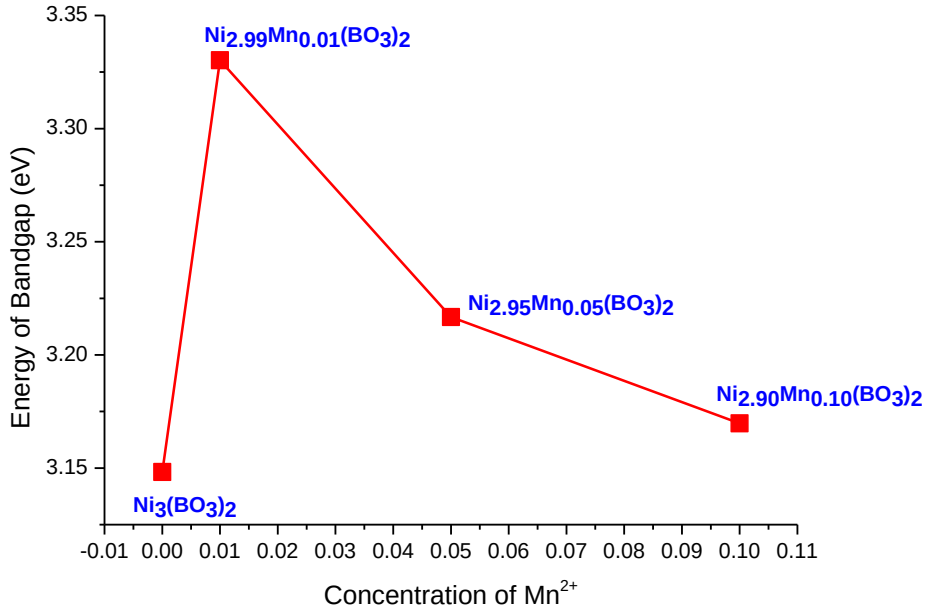

Figure 4.20. Graph of change of $(\alpha h\nu)^2$ relative to hν for the calculation of the forbidden energy range $Ni_3(BO_3)_2$: $0.100Mn^{2+}$

4.4.3. Calculation and Comparison of the Band Gap Energy Intervals of $Ni_3(BO_3)_2$: Mn^{2+}, RE^{3+} (RE = Ce, Eu, and Tb) Compounds

After determining the optimum value for the doping concentration of manganese (II) metal, cerium (III), europium (III) and terbium (III) were added to the material as auxiliary additives in different ratios and the changes on ultraviolet absorption properties were investigated.

Optical method was used to determine the forbidden energy range of doped compounds and graphs of change of $(\alpha h\nu)^2$ versus $h\nu$ were plotted. In these graphs, the forbidden energy ranges of these compounds are obtained from the points where the linear part intersects the energy axis. As a result of the evaluation of the absorption spectra, it was observed that there was a decrease in the forbidden energy intervals when the amount of cerium increased. As the amount of europium and terbium increased an increase in these energy values followed by a decrease.

Fig. 4.21, Fig. 4.22 and Fig. 4.23 were used to determine the forbidden energy ranges for $Ni_3(BO_3)_2$: $0.010Mn^{2+}$ compounds doped with cerium (III) rare earth metal and Eg = 3.160 for x = 0.005 molar, Eg = 3,150 for x = 0.01 molar, and Eg = 3.141 for x = 0.02 molar values were found.

A comparison of the forbidden energy ranges of $Ni_3(BO_3)_2$: $0.010Mn^{2+}$, Ce^{3+} (x = 0.000, 0.005, 0.010, 0.020) is given in Figure 4.24.

Figure 4.25, Figure 4.26 and Figure 4.27 show the change graphs of $(\alpha h\nu)^2$ versus $h\nu$ for europium (III) rare earth metal doped $Ni_3(BO_3)_2$: $0.010Mn^{2+}$ compounds. By using these graphs, the forbidden energy ranges for the europium side contribution were determined and Eg = 3.362 for x = 0.005 molar, Eg = 3.345 for x = 0.01 molar and Eg = 3.329 for x = 0.02 molar values were found.

Comparison of the forbidden energy ranges of $Ni_3(BO_3)_2$: $0.010Mn^{2+}$, xEu^{3+} (x = 0.000, 0.005, 0.010, 0.020) is shown on the graph in Figure 4.28.

In Figure 4.29 Figure 4.30 and Figure 4.31, plotted change graphs $(\alpha h\nu)^2$ versus $h\nu$ for terbium (III) rare earth metal doped $Ni_3(BO_3)_2$: $0.010Mn^{2+}$ compounds are given. Forbidden energy ranges (Eg) of terbium-doped compounds were determined by fitting the curves in these graphs. The Eg = 3.341, 3.328 and 3.325 eV values were found for x = 0.005, 0.01 and 0.02 molar values of terbium respectively. Comparison of the forbidden energy ranges of $Ni_3(BO_3)_2$: 0.010 Mn^2

$^{+}$, xTb^{3+} (x = 0.000, 0.005, 0.010, 0.020) is presented graphically in Figure 4.32.

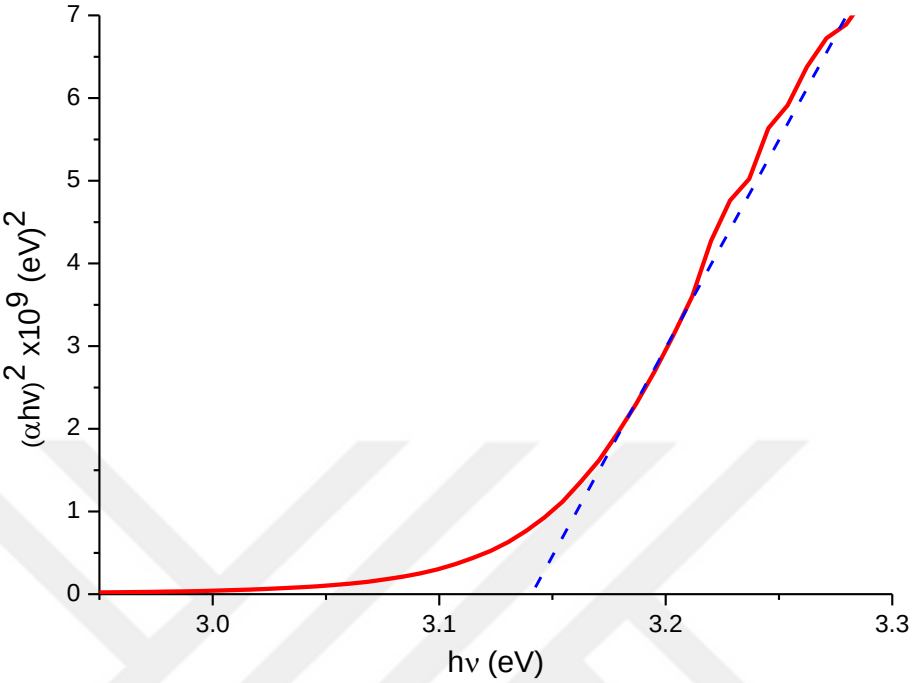

Figure 4.21. Graph of change of $(\alpha h\nu)^2$ relative to hν for the calculation of the forbidden energy range of $Ni_3(BO_3)_2$: $0.010Mn^{2+}$, $0.005Ce^{3+}$

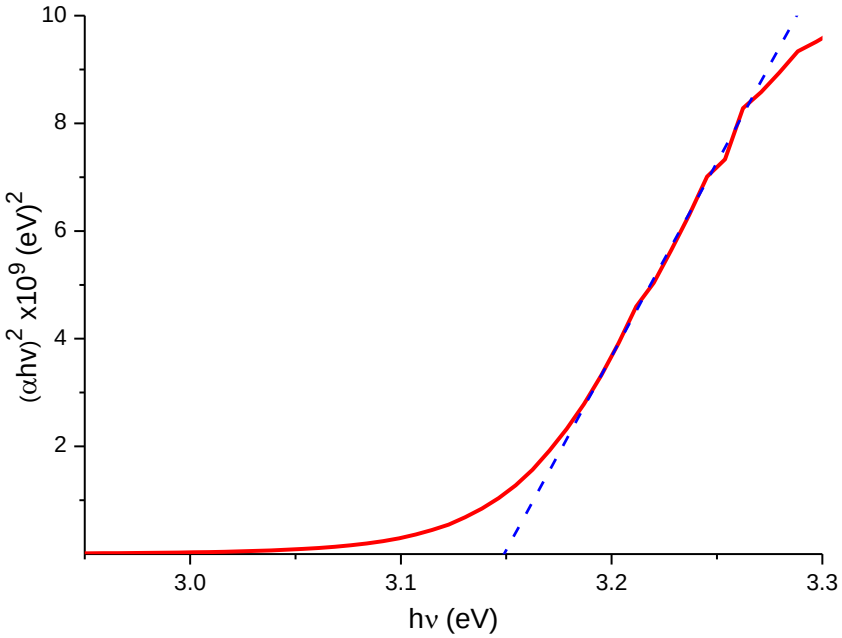

Figure 4.22. Graph of change of $(\alpha h\nu)^2$ relative to hν for the calculation of the forbidden energy range of $Ni_3(BO_3)_2$: $0.010Mn^{2+}$, $0.010Ce^{3+}$

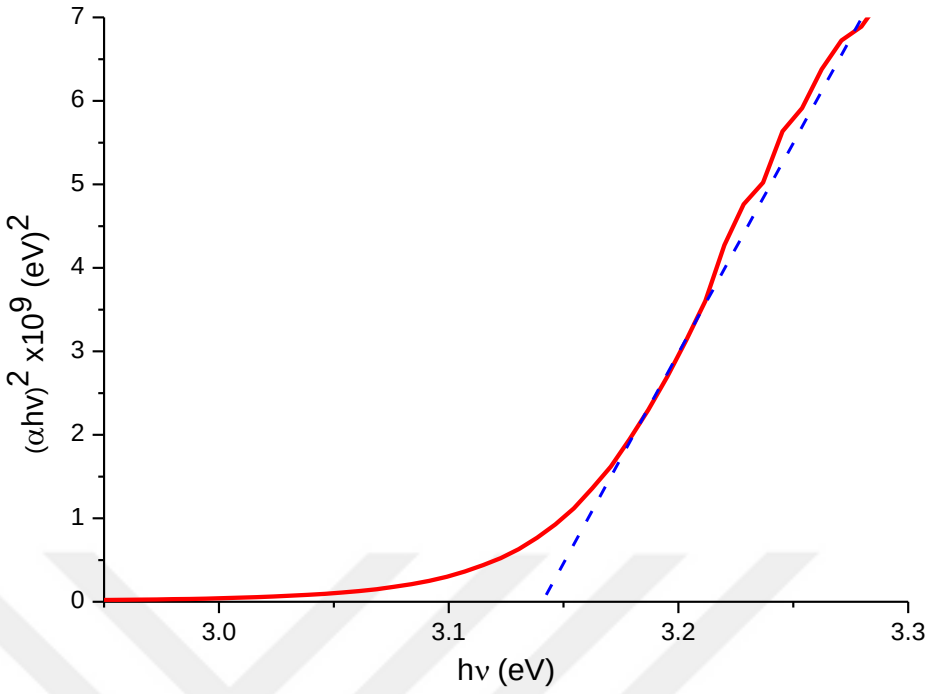

Figure 4.23. Graph of change of $(\alpha h\nu)^2$ relative to hν for the calculation of the forbidden energy range of $Ni_3(BO_3)_2$: $0.010Mn^{2+}$, $0.02Ce^{3+}$

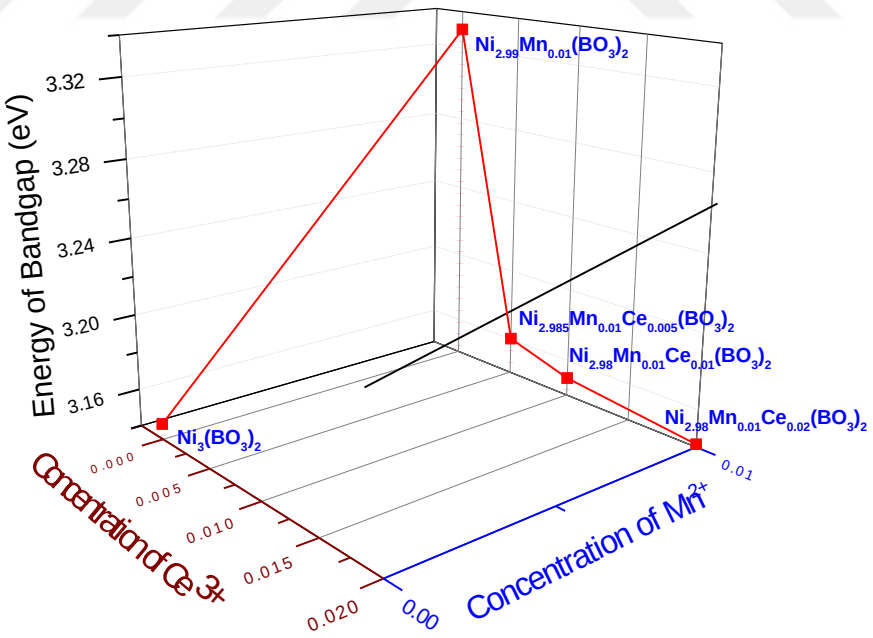

Figure 4.24. Comparison of forbidden energy ranges of $Ni_3(BO_3)_2$: $0.010Mn^{2+}$, $\mathbf{x}Ce^{3+}$ (**x**= 0.000, 0.005, 0.010, 0.020) compounds

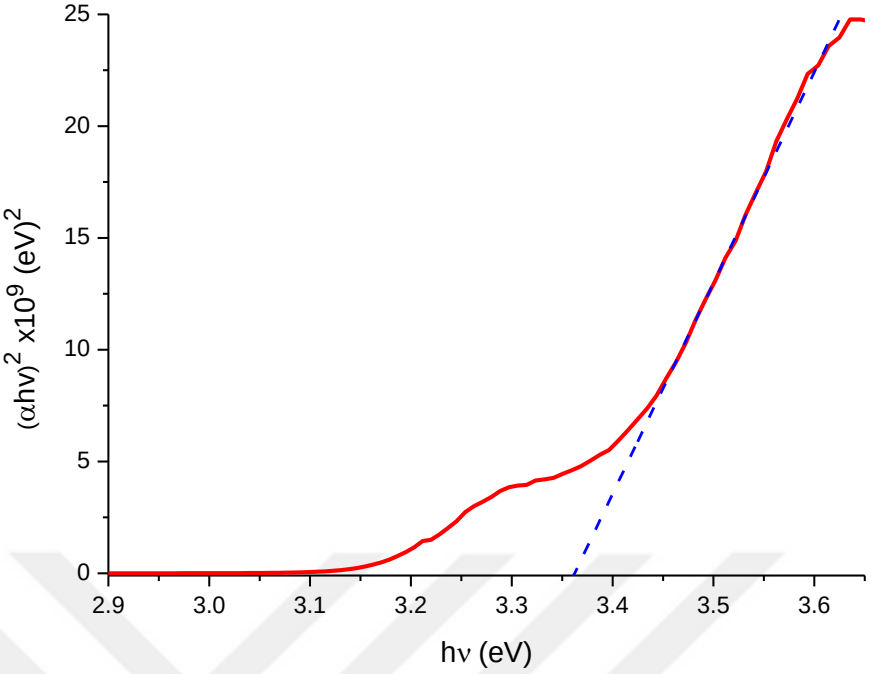

Figure 4.25. Graph of change of $(\alpha h\nu)^2$ relative to hν for the calculation of the forbidden energy range of $Ni_3(BO_3)_2$: $0.010Mn^{2+}$, $0.005Eu^{3+}$

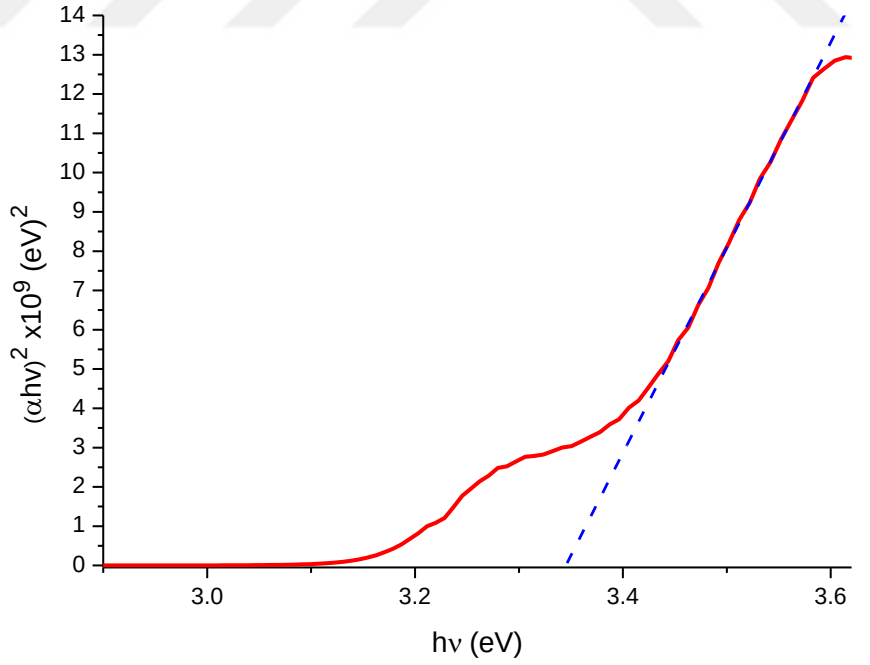

Figure 4.26. Graph of change of $(\alpha h\nu)^2$ relative to hν for the calculation of the forbidden energy range of $Ni_3(BO_3)_2$: $0.010Mn^{2+}$, $0.010Eu^{3+}$

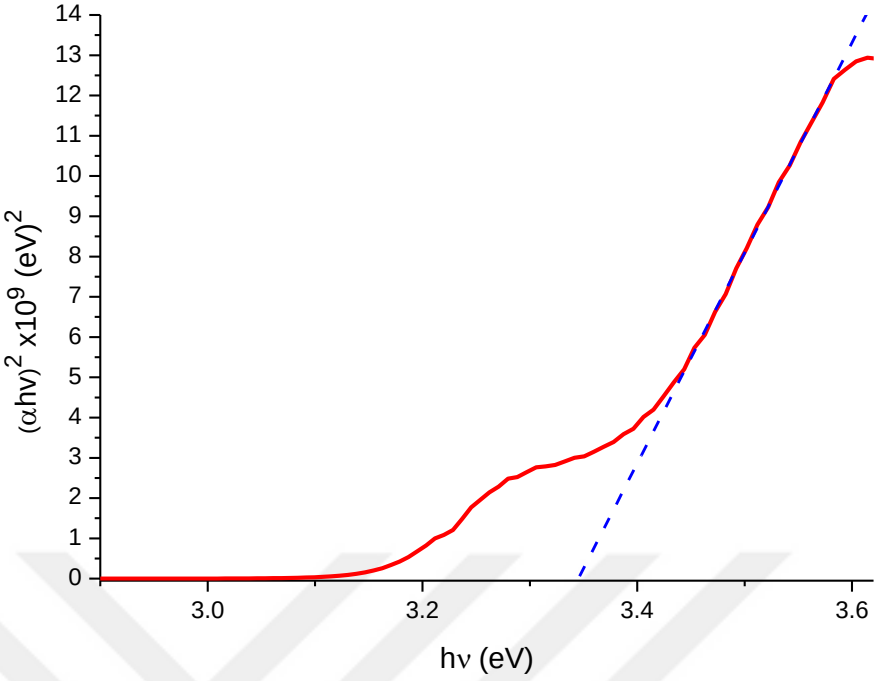

Figure 4.27. Graph of change of $(\alpha h\nu)^2$ relative to hν for the calculation of the forbidden energy range of $Ni_3(BO_3)_2$: $0.010Mn^{2+}$, $0.020Eu^{3+}$

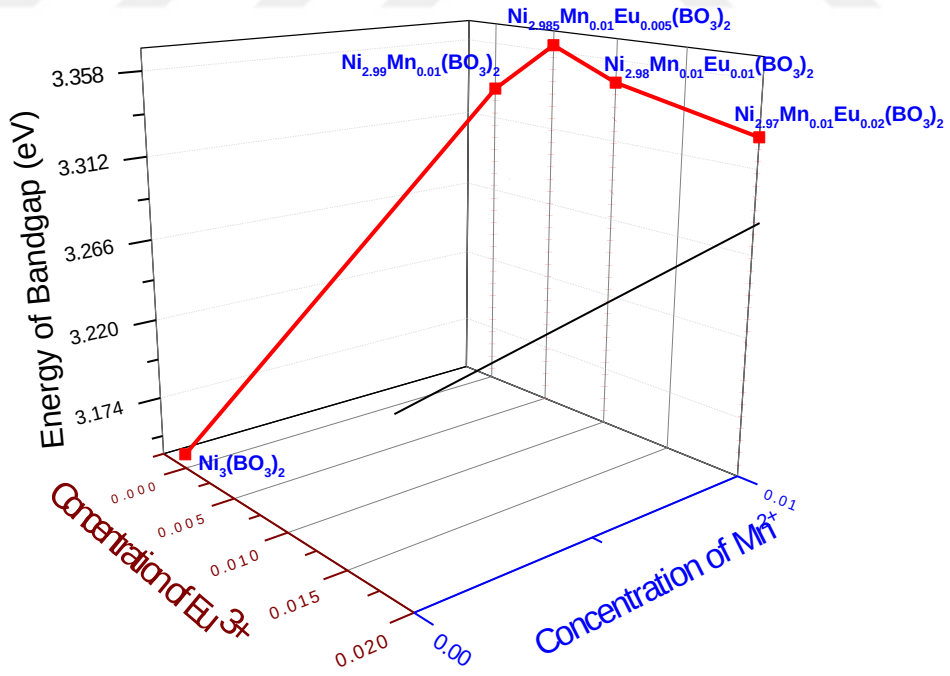

Figure 4.28. Comparison of forbidden energy ranges of $Ni_3(BO_3)_2$: $0.010Mn^{2+}$, $\mathbf{x}Eu^{3+}$ (**x**= 0.000, 0.005,0.010, 0.020) compounds

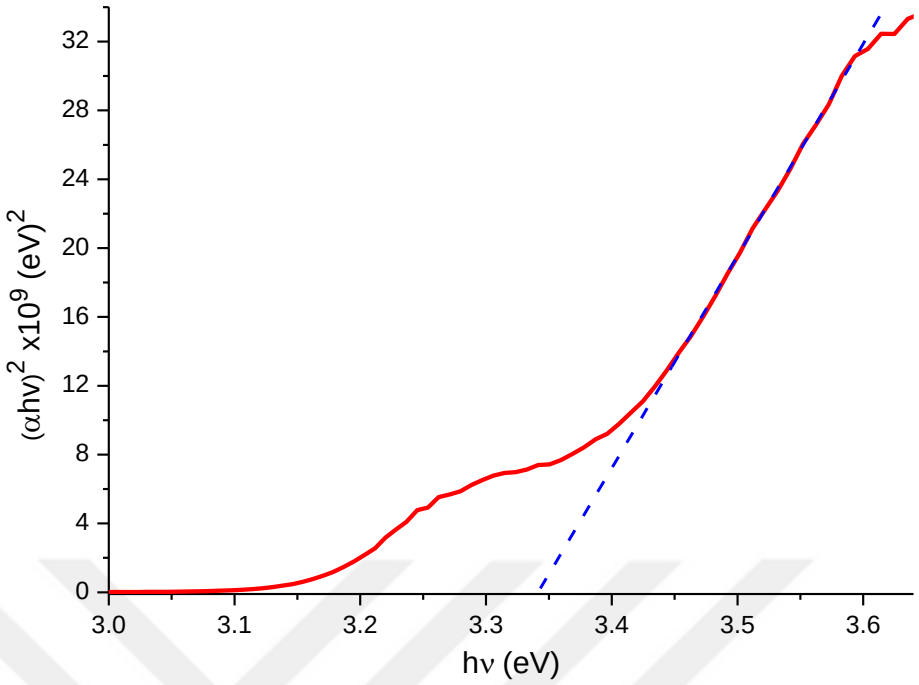

Figure 4.29. Graph of change of $(\alpha h\nu)^2$ relative to hν for the calculation of the forbidden energy range of $Ni_3(BO_3)_2$: $0.010Mn^{2+}$, $0.005Tb^{3+}$

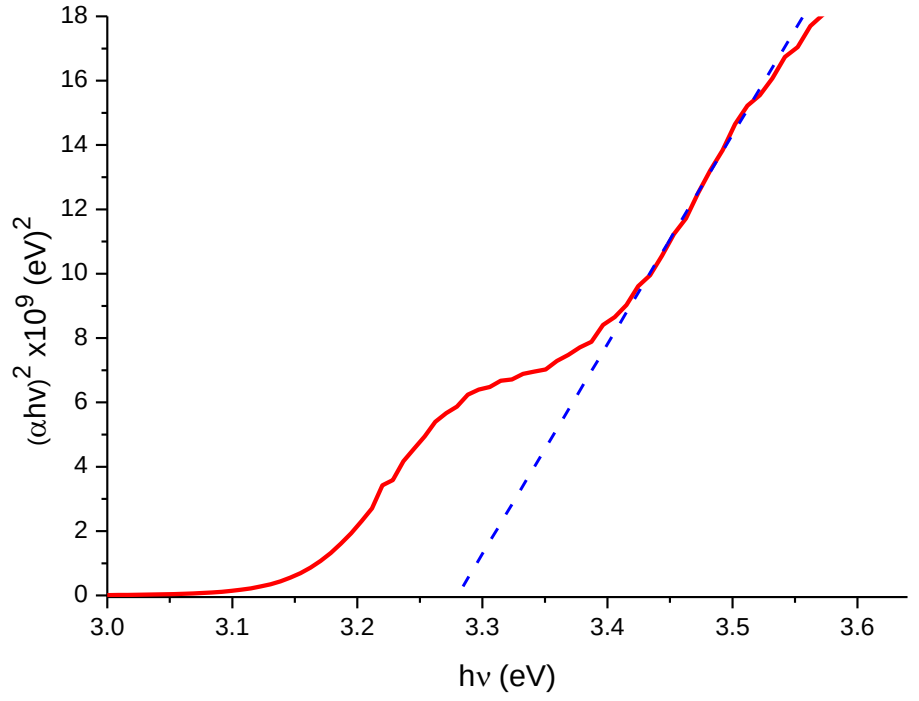

Figure 4.30. Graph of change of $(\alpha h\nu)^2$ relative to hν for the calculation of the forbidden energy range of $Ni_3(BO_3)_2$: $0.010Mn^{2+}$, $0.010Tb^{3+}$

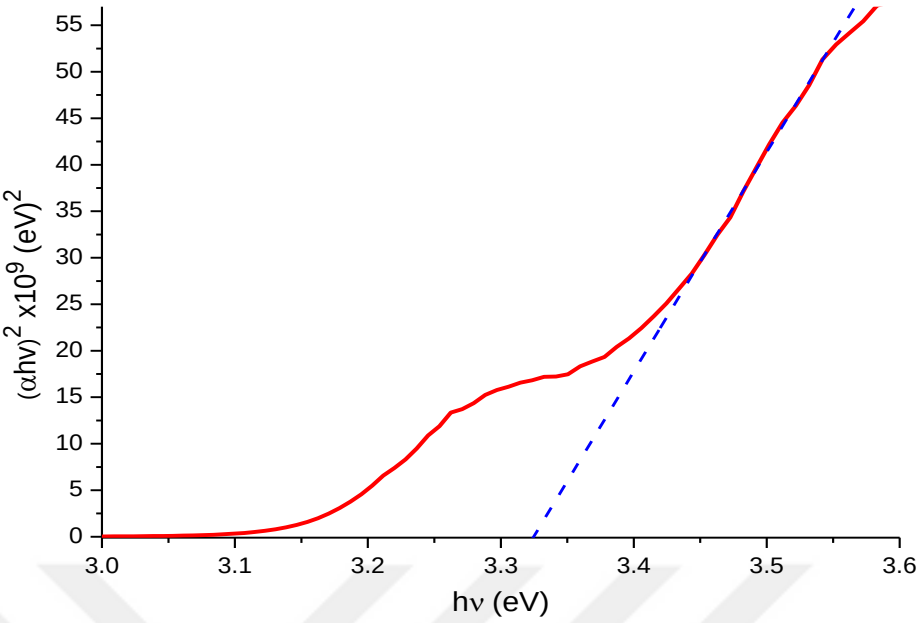

Figure 4.31. Graph of change of $(\alpha h\nu)^2$ relative to hν for the calculation of the forbidden energy range of $Ni_3(BO_3)_2$: $0.010Mn^{2+}$, $0.020Tb^{3+}$

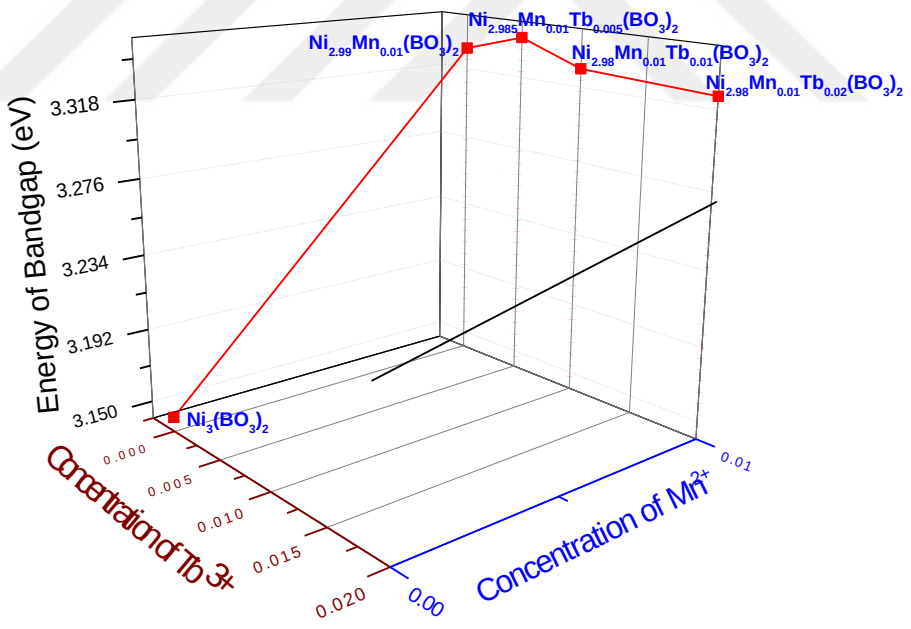

Figure 4.32. Comparison of the forbidden energy ranges of $Ni_3(BO_3)_2$: $0.010Mn^{2+}$, xTb^{3+} (x = 0.000, 0.005, 0.010, 0.020)

4.5. Jana2006 Analysis of Synthesized Materials and Calculation of Crystal Size, Density, Surface Area Using Debye-Scherrer Equation

4.5.1. Jana2006 Analysis of $Ni_3(BO_3)_2$: xMn^{2+} (0.00, 0.01, 0.05, 0.10) and Calculation of Crystal Size and Density, Surface Area Using Debye-Scherrer Equation

When the Jana2006 analysis results of 0.003, 0.01, 0.05 and 0.10 manganese (II) doped $Ni_3(BO)_2$ compounds given in Figure 4.33 were examined to determine the optimum concentration, the GOF values are 1.16, 1.18, 1.67 and 4.58 respectively. The most compatible data is obtained when 0.010 manganese (II) is added to the compound and it is understood that the harmony began to deteriorate while the amount of manganese increases. Detailed Jana2006 analysis results are given in Table 4.3.

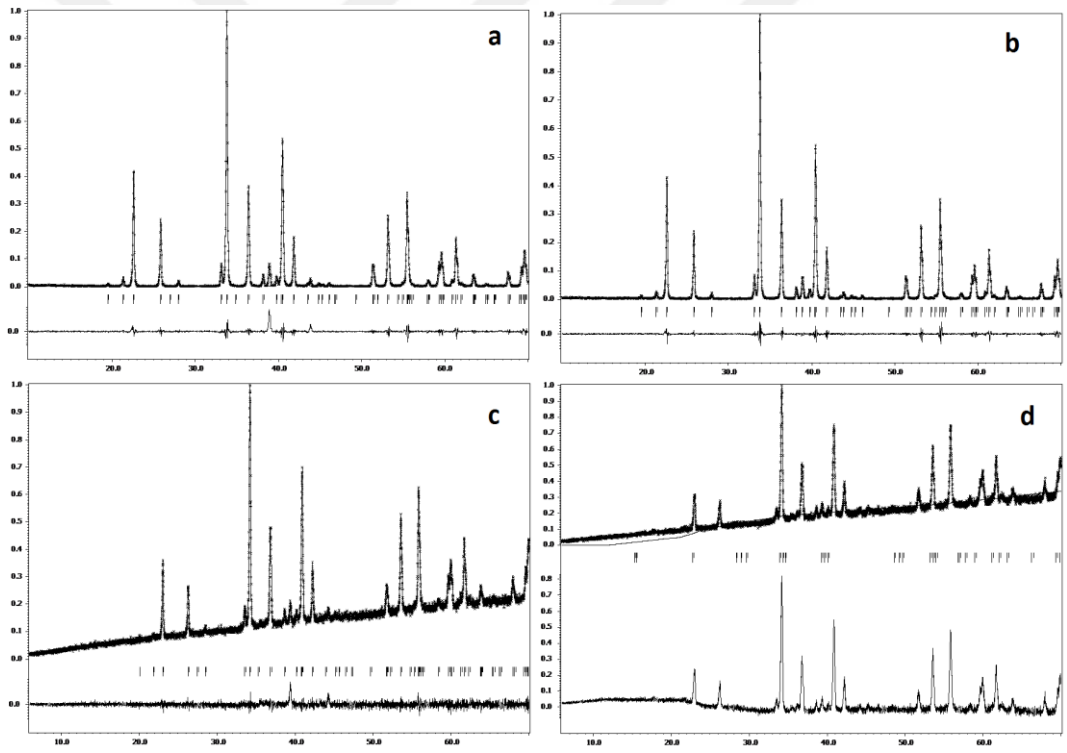

Figure 4.33. Jana2006 analysis patterns for $Ni_3(BO_3)_2$: xMn^{2+} (0.00, 0.01, 0.05, 0.10) materials

Table 4.3. $Ni_3 (BO_3)_2$: xMn^{2+} (0.00, 0.01, 0.05, 0.10) Jana2006 detailed analysis results for the materials

Products	**$Ni_3(BO_3)_2$**	**$Ni_3(BO_3)_2$: 0.01Mn^{2+}**	**$Ni_3(BO_3)_2$: 0.05Mn^{2+}**	**$Ni_3(BO_3)_2$: 0.10Mn^{2+}**
Diffractometer	Rigaku	Rigaku	Rigaku	Rigaku
Radiation type	Cu Kα	Cu Kα	Cu Kα	Cu Kα
Monochromator	Graphite	Graphite	Graphite	Graphite
Wavelength (Å)	1.5405	1.5405	1.5405	1.5405
Refined profile range($^o2\theta$)	10.00-70.00	10.00-70.00	10.00-70.00	10.00-70.00
Step size ($^o2\theta$)	0.02	0.02	0.02	0.02
Material	Powder crystal	Powder crystal	Powder crystal	Powder crystal
Symmetry	orthorhombic	orthorhombic	orthorhombic	orthorhombic
Space group	Pnmn	Pnmn	Pnmn	Pnmn
a (Å)	5.3974	5.3989	5.4135	5.3960
b (Å)	4.4598	4.4605	4.4714	4.4590
c (Å)	8.3007	8.3033	8.3271	8.2970
α (^{o} degree)	90.000	90.000	90.000	90.000
β (^{o} degree)	90.000	90.000	90.000	90.000
δ (^{o} degree)	90.000	90.000	90.000	90.000
GOF	1.16	1.18	1.67	4.58
R_P	4.05	8.28	9.82	14.84
R_{WP}	5.61	12.87	18.13	22.96
V	199.8	200.0	201.6	202.1

GOF, R_P, R_{WP}: *agreement factors,* ***V:*** *volume*

4.5.2. Jana 2006 Analysis $Ni_3(BO_3)_2$: of Mn^{2+}, RE^{3+} (RE = Ce, Eu, and Tb) Compounds and Calculation of Crystal Size, Density, Surface Area Using Debye-Scherrer Equation

Jana2006 patterns of materials obtained by adding manganese (II) metal together with cerium (III), europium (III) and terbium (III) rare earth metals are given in Figures 4.34-4.35. The GOF values of cerium-doped $Ni_3(BO_3)_2$: $0.010Mn^{2+}$, xCe^{3+} (x = 0.005, 0.010, 0.020) were 1.70, 1.86 and 2.01, respectively. The GOF values of the compounds europium doped $Ni_3(BO_3)_2$: $0.010Mn^{2+}$, xEu^{3+} (x = 0.005, 0.010, 0.020) were 1.63, 1.68 and 1.73 and terbium doped $Ni_3(BO_3)_2$: $0.010Mn^{2+}$, xTb^{3+} (x = 0.005, 0.010, 0.020) were found to be 1.67, 1.78 and 1.91, respectively. Our results show that the materials we synthesize are compatible with kotoite structure. The XRD patterns of the doped compounds obtained according to Jana 2006 data coincide with the kotoite structure. When the GOF data are examined, values close to 1 have been obtained, which shows that the adaptation to the kotoite structure is very good. Detailed Jana2006 analysis results are given in Table 4.4-4.6.

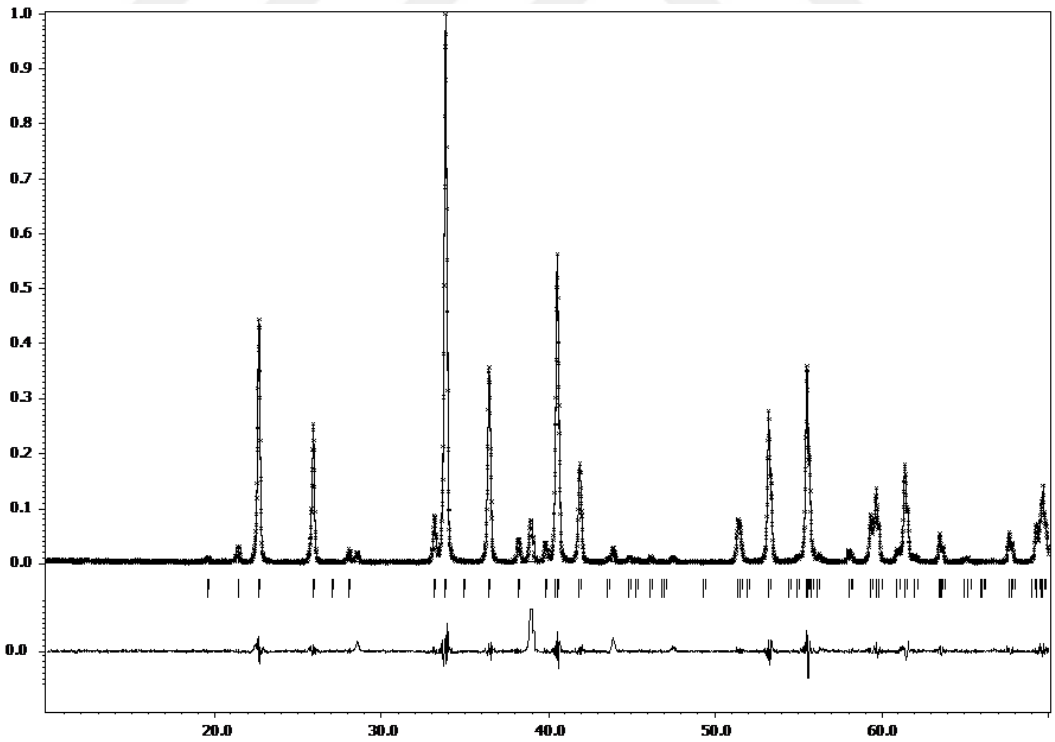

Figure 4.34. Jana2006 analysis pattern of $Ni_3(BO_3)_2$: $0.010Mn^{2+}$, $0.005Ce^{3+}$

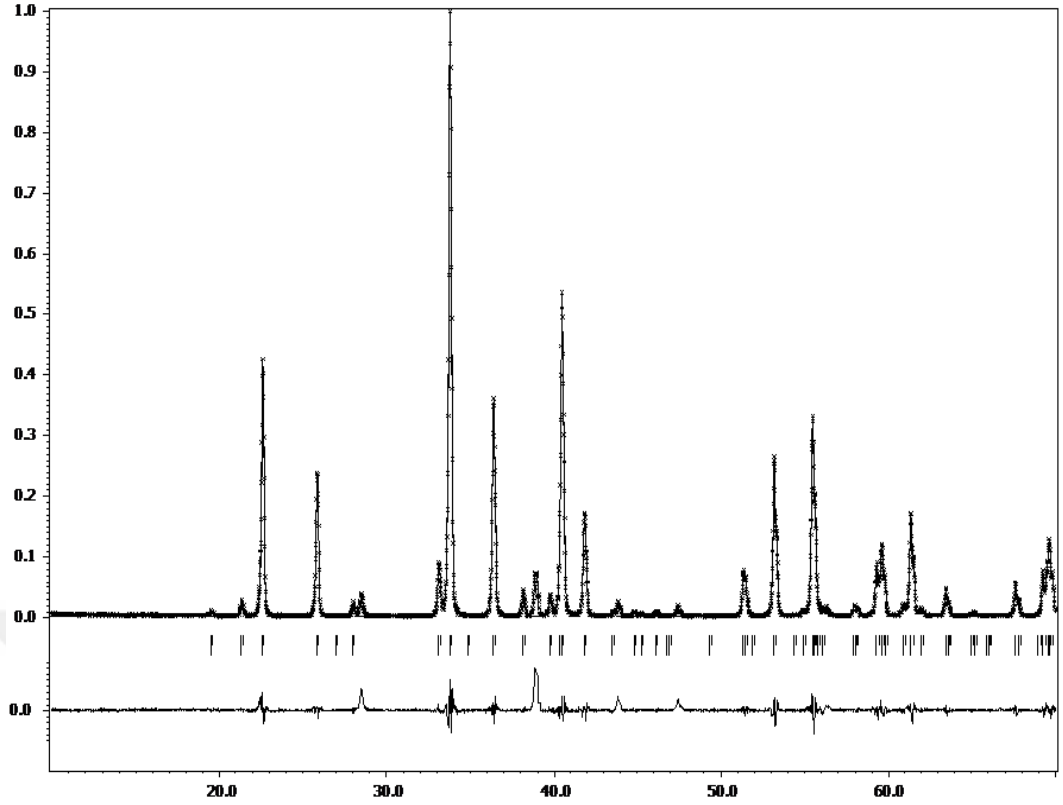

Figure 4.35. Jana2006 analysis pattern of $Ni_3(BO_3)_2$: $0.010Mn^{2+}$, $0.010Ce^{3+}$

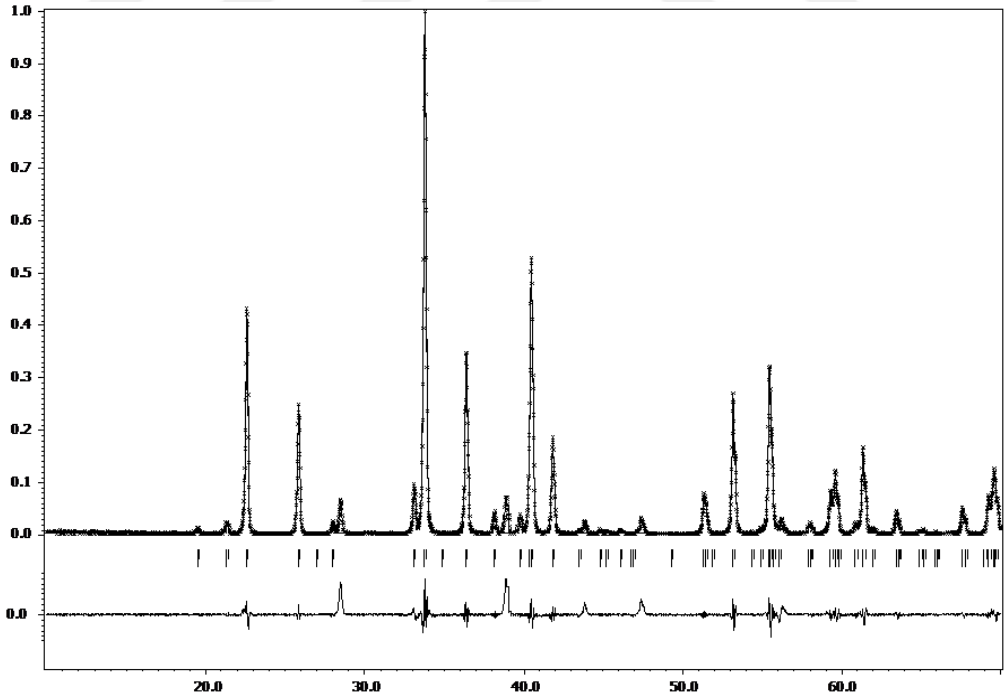

Figure 4.36. Jana2006 analysis pattern of $Ni_3(BO_3)_2$: $0.010Mn^{2+}$, $0.020Ce^{3+}$

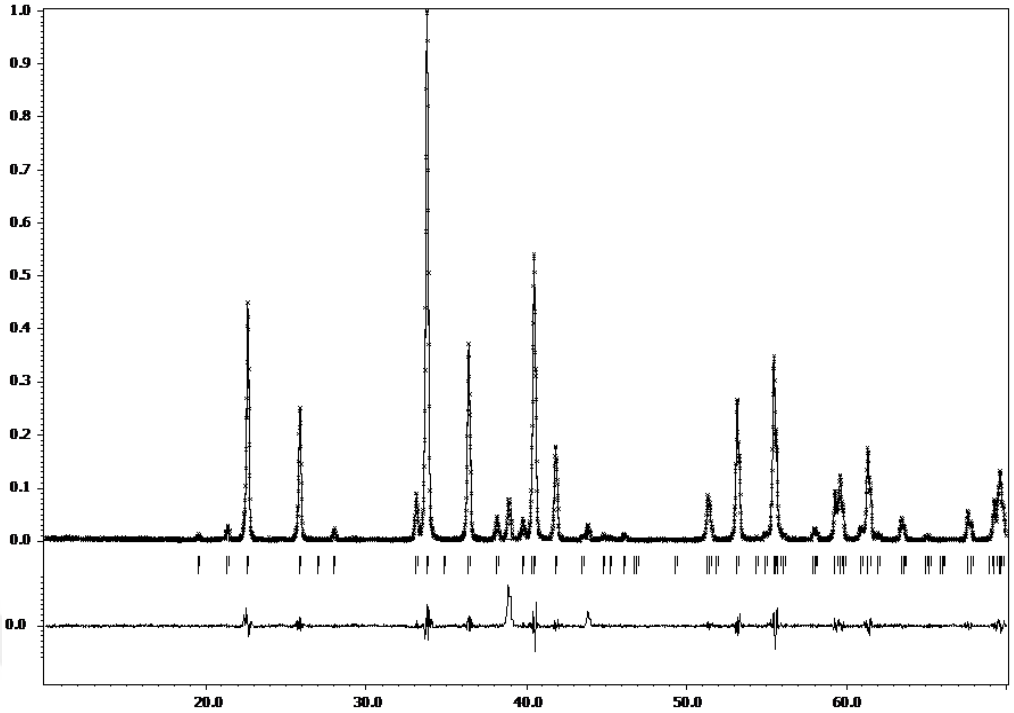

Figure 4.37. Jana2006 analysis pattern of $Ni_3(BO_3)_2$: $0.010Mn^{2+}$, $0.005Eu^{3+}$

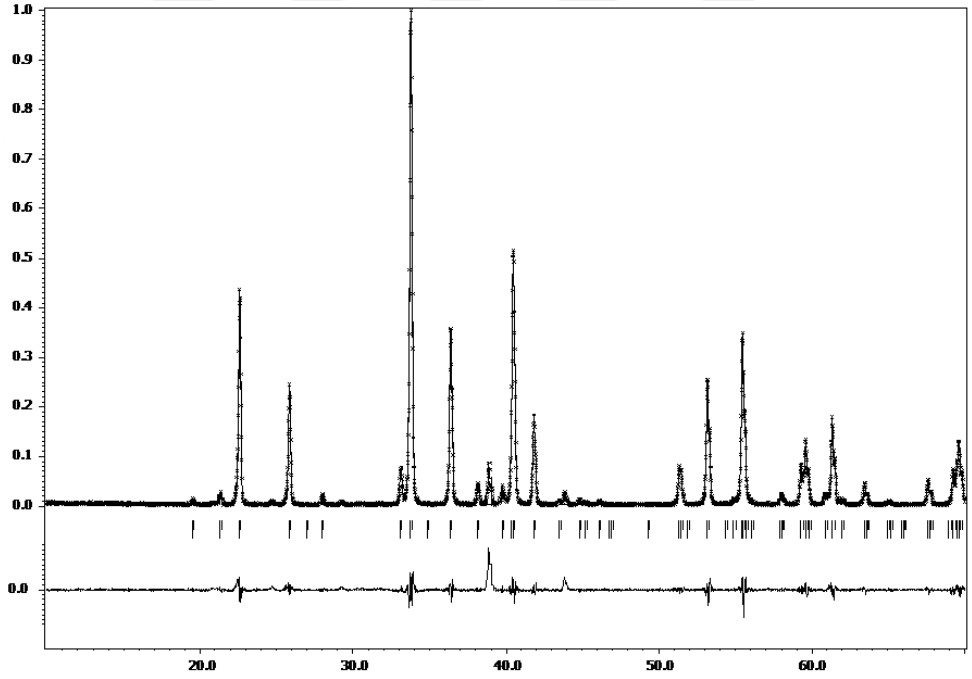

Figure 4.38. Jana2006 analysis pattern of $Ni_3(BO_3)_2$: $0.010Mn^{2+}$, $0.010Eu^{3+}$

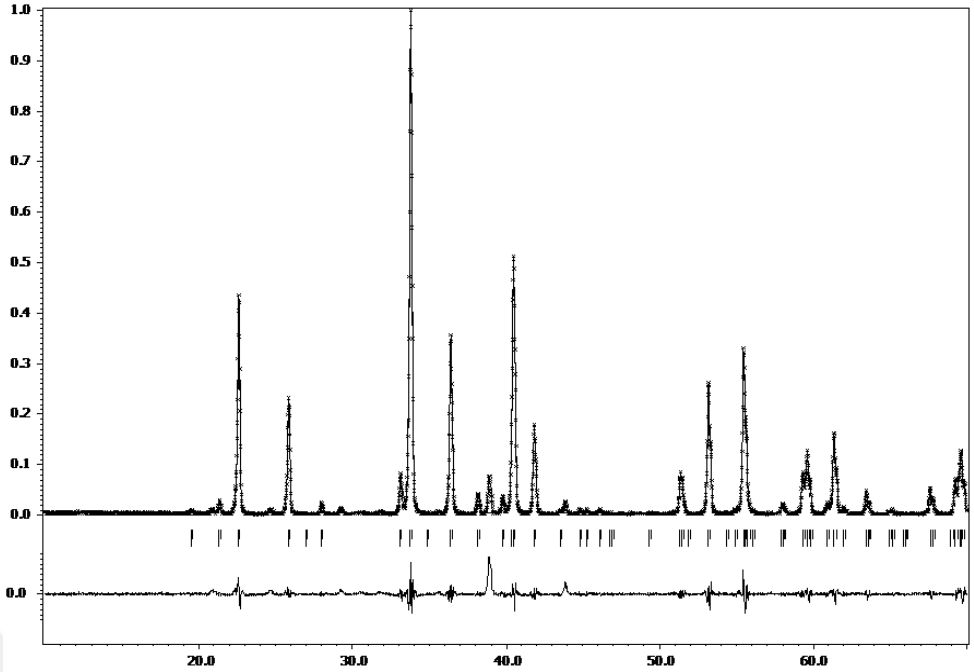

Figure 4.39. Jana2006 analysis pattern of $Ni_3(BO_3)_2$: $0.010Mn^{2+}$, $0.020Eu^{3+}$

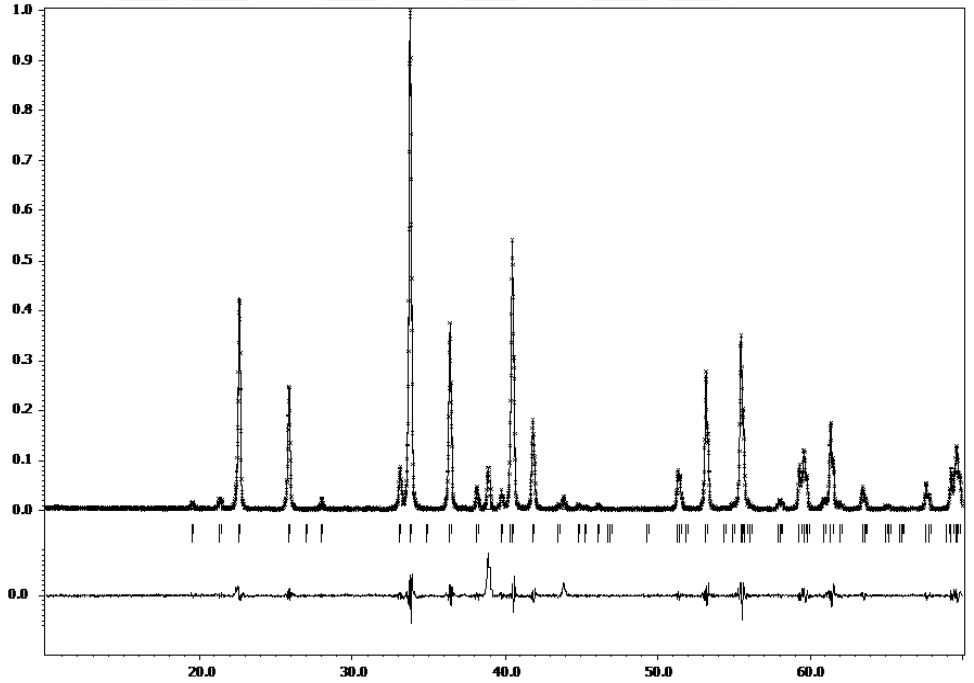

Figure 4.40. Jana2006 analysis pattern of $Ni_3(BO_3)_2$: $0.010Mn^{2+}$, $0.005Tb^{3+}$

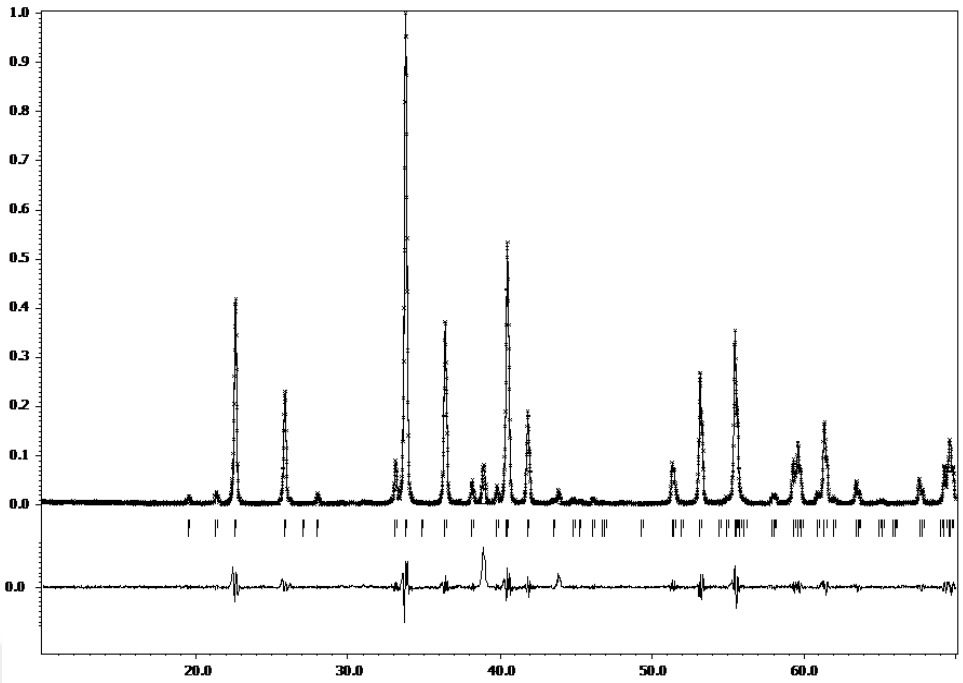

Figure 4.41. Jana2006 analysis pattern of $Ni_3(BO_3)_2$: $0.010Mn^{2+}$, $0.010Tb^{3+}$

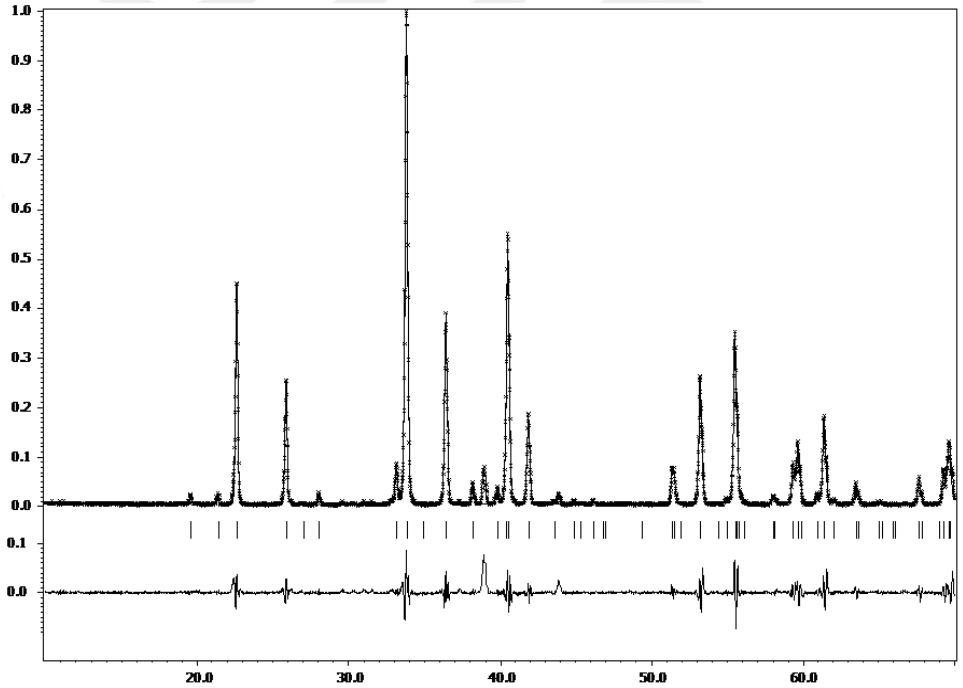

Figure 4.42. Jana2006 analysis pattern of $Ni_3(BO_3)_2$: $0.010Mn^{2+}$, $0.020Tb^{3+}$

Table 4.4. Detailed Jana2006 analysis results of $Ni_3(BO_3)_2$: $0.010Mn^{2+}$,xCe^{3+} (x= 0.000, 0.005, 0.010, 0.020) synthesized materials

Materials	**$Ni_3(BO_3)_2$: $0.010Mn^{2+}$**	**$Ni_3(BO_3)_2$: $0.010Mn^{2+}$, $0.005Ce^{3+}$**	**$Ni_3(BO_3)_2$: $0.010Mn^{2+}$, $0.010Ce^{3+}$**	**$Ni_3(BO_3)_2$: $0.010Mn^{2+}$, $0.020Ce^{3+}$**
Diffractometre	Rigaku	Rigaku	Rigaku	Rigaku
Radiation type	Cu Kα	Cu Kα	Cu Kα	Cu Kα
Monochromator	Graphite	Graphite	Graphite	Graphite
Wavelength (Å)	1.5405	1.5405	1.5405	1.5405
Refined profile range($^o2\theta$)	10.00-70.00	10.00-70.00	10.00-70.00	10.00-70.00
Step size ($^o2\theta$)	0.02	0.02	0.02	0.02
Malzeme	Powder crystal	Powder crystal	Powder crystal	Powder crystal
Symmetry	orthorhombic	Orthorhombic	orthorhombic	orthorhombic
Uzay grubu	Pnmn	Pnmn	Pnmn	Pnmn
a (Å)	5.3989	5.4000	5.3987	5.3976
b (Å)	4.4605	4.4615	4.4605	4.4597
c (Å)	8.3033	8.3049	8.3032	8.3016
α (^{o} degree)	90.000	90.000	90.000	90.000
β (^{o} degree)	90.000	90.000	90.000	90.000
δ (^{o} degree)	90.000	90.000	90.000	90.000
GOF	1.18	1.70	1.86	2.01
R_P	8.28	10.26	11.16	12.37
R_{WP}	12.87	18.94	20.47	22.65
V	200.0	199.8	200.0	200.1

GOF, R_P, R_{WP}: *agreement factors,* ***V:*** *volume*

Table 4.5. Detailed Jana2006 analysis results of $Ni_3(BO_3)_2$: $0.010Mn^{2+}$,xEu^{3+} (x= 0.000, 0.005, 0.010, 0.020) synthesized materials

Materials	**$Ni_3(BO_3)_2$: $0.010Mn^{2+}$**	**$Ni_3(BO_3)_2$: $0.010Mn^{2+}$, $0.005Eu^{3+}$**	**$Ni_3(BO_3)_2$: $0.010Mn^{2+}$, $0.010Eu^{3+}$**	**$Ni_3(BO_3)_2$: $0.010Mn^{2+}$, $0.020Eu^{3+}$**
Diffractometre	Rigaku	Rigaku	Rigaku	Rigaku
Radiation type	Cu Kα	Cu Kα	Cu Kα	Cu Kα
Monochromator	Graphite	Graphite	Graphite	Graphite
Wavelength (Å)	1.5405	1.5405	1.5405	1.5405
Refined profile range($^o2\theta$)	10.00-70.00	10.00-70.00	10.00-70.00	10.00-70.00
Step size ($^o2\theta$)	0.02	0.02	0.02	0.02
Malzeme	Powder crystal	Powder crystal	Powder crystal	Powder crystal
Symmetry	orthorhombic	orthorhombic	orthorhombic	orthorhombic
Uzay grubu	Pnmn	Pnmn	Pnmn	Pnmn
a (Å)	5.3989	5.3994	5.3991	5.3985
b (Å)	4.4605	4.4607	4.4603	4.4599
c (Å)	8.3033	8.3036	8.3032	8.3015
α (^{o} degree)	90.000	90.000	90.000	90.000
β (^{o} degree)	90.000	90.000	90.000	90.000
δ (^{o} degree)	90.000	90.000	90.000	90.000
GOF	1.18	1.63	1.68	1.73
R_P	8.28	10.17	10.27	11.33
R_{WP}	12.87	18.16	18.60	19.59
V	200.0	199.9	200.0	200.0

GOF, R_P, R_{WP}: *agreement factors,* ***V:*** *volume*

Table 4.6. Detailed Jana2006 analysis results of $Ni_3(BO_3)_2$: $0.010Mn^{2+}$,xTb^{3+} (x= 0.000, 0.005, 0.010, 0.020) synthesized materials

Materials	**$Ni_3(BO_3)_2$: $0.010Mn^{2+}$**	**$Ni_3(BO_3)_2$: $0.010Mn^{2+}$, $0.005Tb^{3+}$**	**$Ni_3(BO_3)_2$: $0.010Mn^{2+}$, $0.010Tb^{3+}$**	**$Ni_3(BO_3)_2$: $0.010Mn^{2+}$, $0.020Tb^{3+}$**
Diffractometre	Rigaku	Rigaku	Rigaku	Rigaku
Radiation type	Cu Kα	Cu Kα	Cu Kα	Cu Kα
Monochromator	Graphite	Graphite	Graphite	Graphite
Wavelength (Å)	1.5405	1.5405	1.5405	1.5405
Refined profile range($^o2\theta$)	10.00-70.00	10.00-70.00	10.00-70.00	10.00-70.00
Step size ($^o2\theta$)	0.02	0.02	0.02	0.02
Malzeme	Powder crystal	Powder crystal	Powder crystal	Powder crystal
Symmetry	orthorhombic	Orthorhombic	Orthorhombic	orthorhombic
Uzay grubu	Pnmn	Pnmn	Pnmn	Pnmn
a (Å)	5.3989	5.3986	5.3987	5.3989
b (Å)	4.4605	4.4603	4.4604	4.4610
c (Å)	8.3033	8.3029	8.3032	8.3031
α (^{o} degree)	90.000	90.000	90.000	90.000
β (^{o} degree)	90.000	90.000	90.000	90.000
δ (^{o} degree)	90.000	90.000	90.000	90.000
GOF	1.18	1.67	1.78	1.91
R_P	8.28	10.44	11.91	13.86
R_{WP}	12.87	18.28	19.60	21.31
V	200.0	199.9	200.0	200.1

GOF, R_P, R_{WP}: *agreement factors,* ***V:*** *volume*

5. CONCLUSIONS AND RECOMMENDATIONS

In this study, the preparation of undoped and doped nickel orthoborates were conducted by the high temperature solid state method. The doped nickel orthoborates were synthesized by adding 0.01 molar concentration of manganese (II) metal to nickel borate compound together with cerium (III), europium (III) and terbium (III) rare earth metals at 0.005, 0.010 and 0.020 molar concentrations. The $Ni_3(BO_3)_2$: $0.01Mn^{2+}$ xRE^{3+} (RE = Ce, Eu, and Tb, x = 0.000, 0.005, 0.010, 0.020) nanosized ceramic powders were also successfully fabricated. The characterization of the obtained compounds was carried out via X-ray Diffraction (XRD), Infrared Spectroscopy (FTIR), UV-Vis diffuse reflectance spectroscopy (DRS) and Thermogravimetric/Differential Thermal Analysis (TG/DTA) method. The optical properties of synthesized manganese metal and cerium, europium and terbium doped nickel borate compounds were examined by using UV-Vis diffuse reflectance spectroscopy (DRS).

In order to determine the forbidden energy intervals, the absorption spectra of the materials obtained and were used in Kubela Munk function to plot the $(\alpha h\nu)^2$ to $h\nu$ graphs at which the points where the linear part cut off the energy axis gives the forbidden energy ranges of these compounds.

In addition, structural analyses were performed by using Jana2006 with the help of X-ray patterns in order to examine the changes in the structure of the nickel borate compound.

The results of this study are as follows:

- According to the X-ray diffractometer results, it was determined that the additives in all synthesized compounds did not affect the phase of nickel orthoborate and all of the obtained compounds were in orthorhombic phases.
- Vibration bands of trigonal BO_3 are observed in infrared spectra of all products obtained in accordance with XRD data.
- The changes in thermal properties were examined comparatively using thermogravimetric analysis-differential thermal analysis (TG/DTA). There were no changes from room temperature to 1380ºC. The endothermic peak at around 1380ºC is thought to be the melting point of nickel borate and

since the additives were only in trace amounts they did not cause a significant decrease in the melting point.

- In the UV-Vis diffuse reflectance spectra of the doped nickel borate compounds, there were two broad absorption bands in the range of 350-550 nm and 650-850 nm. It has been observed that the addition of cerium, europium and terbium elements were caused the reflectance bands to shift to the lower wavelengths from visible to near infrared region. It is also revealed that that the reflectance value decreases to a certain point with increasing amount of rare earth metals and then it starts to increase when the amount of rare earth metal is continued to be increased.

This is explained that the contribution of the additives cause the damping after reaching the maximum absorption value. The highest absorption value is obtained by europium doped compounds, while the highest absorption value is given by x = 0.010 europium doped compounds. Terbium-doped compounds gave the highest absorption value after europium, and the optimum value in terbium was found to be 0.005 doped compound. Cerium doped compounds were found to have lower absorption than other doped compounds.

- The changes of linear absorption coefficient values of the synthesized compounds $Ni_3(BO_3)_2$: xMn^{2+} (x: 0.000, 0.010, 0.050 and 0.100) and $Ni_3(BO_3)_2$: $0.01Mn^{2+}$, xRE^{3+} (RE = Ce, Eu, and Tb, x = 0.000, 0.005, 0.010, 0.020) with wavelength were investigated and the graphs of $(\alpha h\nu)^2$ against $h\nu$ were plotted for each material. Forbidden energy ranges were determined with the help of graphs. Forbidden energy range of materials (Eg) was calculated ;
    a. In $Ni_3(BO_3)_2$: xMn^{2+} (x:0.000, 0.010, 0.050 ve 0.100) compounds, the forbidden energies value are 3.148 eV for x=0.000, 3.330 eV for x=0.010, 3.216 eV for x= 0.050 and 3.170 eV for x=0.100. It was observed that forbidden energy are increased with increasing manganese (II) concentration and then started to decrease.
    b. In $Ni_3(BO_3)_2$: $0.010Mn^{2+}$, xCe^{3+} (x= 0.005, 0.010, 0.020) compounds, the forbidden energies values equal to 3.160 eV for x=0.005, 3.150 eV for x= 0.010 and 3.141 eV for x=0.020. It was also showed that forbidden energy range was decreased with increased Ce (III) concentration.

c. In $Ni_3(BO_3)_2$: $0.010Mn^{2+}$, xEu^{3+} (x= 0.005, 0.010, 0.020) compounds, the forbidden energies are determined to be 3.362 eV for x=0.005, 3.345 eV for x= 0.010 and 3.329 eV for x=0.020. The values were observed to be decreased with the increasing Eu (III) concentration.

d. In $Ni_3(BO_3)_2$: $0.010Mn^{2+}$, xTb^{3+} (x= 0.005, 0.010, 0.020) compounds, the forbidden energies are found at 3.341 eV for x=0.005, 3.328 eV for x= 0.010 and 3.325 eV for x=0.020. It was indicated that forbidden energy range decreased with increasing Tb (III) concentration.

- Jana 2006 analysis of 0.010, 0.050 ve 0,100 molar manganese (II) dopped $Ni_3(BO_3)_2$ compounds were performed and GOF values for 0.010, 0.050 ve 0,100 molar manganese doped synthesized compounds were found 1.16, 1.18, 1.67 and 4.58 respectively. As a result, $Ni_3(BO_3)_2$:$0.010Mn^{2+}$ is decided to be the best material for undopped nickel orthoborate structure by comparison of GOF values.

Jana2006 analyses of $Ni_3(BO_3)_2$: $0.010Mn^{2+}$ compounds obtained by cerium, europium and terbium rare earth metal doped were performed. The GOF values of cerium-doped $Ni_3(BO_3)_2$: $0.010Mn^{2+}$, xCe^{3+} (x = 0.005, 0.010, 0.020) were 1.70, 1.86 and 2.01, respectively; The GOF values of europium-doped $Ni_3(BO_3)_2$: $0.010Mn^{2+}$, xEu^{3+} (x = 0.005, 0.010, 0.020) were 1.63, 1.68 and 1.73 and terbium-doped $Ni_3(BO_3)_2$: $0.010Mn^{2+}$ in 0.005, 0.010 and 0.020 were found to be 1.67, 1.78 and 1.91, respectively. This shows that the materials we obtained are compatible with the kotoite structure.

6. REFERENCES

Vancouver citation system was used in this thesis.

1. Ulutaş, C, Kimyasal Depolama Yöntemiyle Elde Edilmiş MnS İnce Filmlerin Özelliklerine Isısal Tavlamanın Etkisi, Doktora Tezi, Adana, 2009.

2. Güner, S., Amir, Md, Geleri, M., Sertkol, M., Baykal, A., Magneto-optical properties of Mn^{3+} substituted Fe_3O_4 nanoparticles, Ceramics International, 41, 10915–10922, (2015).

3. Beatty, R., The Elements Boron, Newyork:Marshall Cavendish Benchmark pub.,4-6, (2006).

4. Péter, A., Polgar, K., Toth, M., Synthesis and crystallization of lithium-yttriumorthoborate $Li_6Y(BO_3)_3$ phase, Journal of Crystal Growth, 346, 69–74, (2012).

5. Chaminade, J. P., Gravereau, P., Jubera, V., Fouassier, C., A New Family of Lithium Rare-Earth Oxyborates, $LiLn_6O_5(BO_3)_3$ (Ln: Pr-Tm): Crystal Structure of the Gadolinium Phase $LiGd_6O_5(BO_3)_3$. Journal of Solid State Chemistry, 146, 189-196, (1999).

6. Zhang, G., Wu, Y., Fu, P., Wang, G., Liu, H., Fan, G., Chen, C., A new sodium samarium borate $Na_3Sm_2(BO_3)_3$.Journal of Phisics and Chemistry of Solids, 63,145-149, (2002).

7. Wu, L., Zhang, Y., Kong, Y. F., Sun, T. Q., Xu, J. J., Chen, X. L., Structure Determination of Novel orthoborates $NaMgBO_3$: A promising Birefringent Crystal. Inorganic Chemistry, 46, 5207-5211, (2007).

8. Anantharamulu, N., Vijaya, Kumar, B., Rama Devi, V., Vithal, M., Preparation, characterization and spectral studies of $Cr_{1-x}EuBO_3$ (x=0, 0.01, 0.05). Material chemistry and physics, 108, 2-3, 319-324, (2008).

9. Latha Kumari, L., Li, W. Z., Kulkarni, S., Wu, K. H., Chen, W., Wang, C., Vannoy, C. H., Leblanc, R. M., Effect of Surfactants on the Structure and Morphology of Magnesium Borate Hydroxide Nanowhiskers Synthesized by Hydrothermal Route. Nanoscale Res Lett, 5, 149–157, (2010).

10. Cai, G. M., Tao, X. M., Su, L. M., Zheng, F., Yi, D. Q., Chen, X. L., Jin, Z. P., Structure, thermal stability and properties of Li3Sc(BO3)2. Journal of Solid State Chemistry, 184, 115–122, (2011).

11. Li, P., Wang, Z., Yang, Z., Guo, Q., Fu, G., Luminescent Characteristics of $LiSrBO_3$:M (M= Eu^{3+},Sm^{3+},Tb^{3+}, Ce^{3+} ve Dy^{3+}) Phosphor for White Light-Emitting Diode, Materials Research Bulletin, 44, 2068-2071, (2009).

12. Li, P., Wang, Z., Yang, Z., Guo, Q., Li, X., Characteristics of $LiCaBO_3$:M (M= Eu^{3+},Sm^{3+},Tb^{3+}, Ce^{3+} ve Dy^{3+}) Phosphor for White LED, Journal of Luminescence, 130, 222–225, (2010).

13. Pitale, S., Nagpure, I. M.,Kumar, V., Ntwaeaborwa O. M., Terblans, J. J., Swart, H. C., Investigations on the low voltage cathodoluminescence stability and surface chemical behavior using auger and X-ray Photoelectron Spectroscopy on $LiSrBO_3$: Sm^{3+} Phosphor, Materials Research Bulletin, 46, 7, 987-994, (2011).

14. A. Akella, D.A. Keszler, Structure and Eu^{3+} Luminescence of Dibarium Magnesium Orthoborate. Materials Research Bulletin 30, 1, 105-111, (1995).

15. Diaz, A., Keszler, D. A. "Red, Green, and blue Eu^{2+} luminescence in solid-state borates: a structure-property relationship", Materials Research Bulletin 31,147, (1996).

16. Diaz, A., Keszler, D. A. "Eu^{2+} Luminescence in the Borates $X_2Z(BO_3)_2$ (X = Ba, Sr; Z = Mg, Ca)" , Chem. Mater. 9, 2071-2077, (1997).

17. Tian, L., Yu, B. Y., Pyun, C. H., Park, H. L., Mho, S. "New red phosphors $BaZr(BO3)_2$ and $SrAl_2B_2O_7$ doped with Eu3+ for PDP applications", Solid State Communications 129, 43–46, (2004).

18. Ignatovych, M., Holovey, V., Watterich, A., Vidoczy, T., Baranyai, P., Kelemen, A., Chuiko, O. "Luminescence characteristics of Cu- and Eu-doped Li2B4O7", Radiation Measurements, 38, 567 – 570, (2004).

19. Berezovskaya, I. V., Efryushina, N. P., Rodnyi, P. A., Voloshinovskii, A. S., Dotsenko, V. P. "Luminescence of Calcium Orthoborate Doped by Ce^{3+} Ions", Optics and Spectroscopy, 101, 6, 902–905, (2006).

20. Liu, L. Y., Zhang, Y. L., Hao, J. Q., Li, C. Y., Tang, Q., Zhang, C. X., Su, Q. (2006). "Thermoluminescence studies of rare earth doped $Sr_2Mg(BO_3)_2$ phosphor", Materials Letters 60, 639–642.

21. Gou,J., Wang, Y., Li, F. "Excitation energy dependent chromaticity of $BaZr(BO_3)_2$: Eu", Journal of Luminescence, 127, 327–331, (2007).

22. Lin, H., Liang, H., Han, B., J., Zhong, Q., Su. "Luminescence and site occupancy of Ce^{3+} in $Ba_2Ca(BO_3)_2$", Physical Review B 76, 035117, (2007).

23. Nagpure, P. A., Omanwar, S. K. "Synthesis and luminescence characteristics of terbium(III) activated $NaSrBO_3$ ", Journal of Rare Earths, 30, 9, 856, (2012).

24. Akhamanova, M. V., Investigation of The Structure of Native Borates by Infrared Absorption Spectroscopy. Zhurnal Strukturnoi Khimii, 3, 1, 28-34, (1961).

25. Ternane, R., Cohen-Adad, M. T., Panczer, G., Goutaudier, C., Kbir-Ariguib, N., Trabelsi-Ayedi, M., Florian, P., and Massiot, D., Introduction of boron in hydroxyapatite: synthesis and structural characterization. Journal of Alloys and Compounds, 333, 62–71, 2002.

26. Lakshminarayana, G., and Buddhudu, S., Spectral analysis of Cu^{2+}: B_2O_3–ZnO–PbO glasses. Spectrochimica Acta Part A, 62, 364–371, 2005.

27. Tukia, M., Hölsä, J., Lastusaari, M., Niittykoski, J., 2005, Eu^{3+} doped rare earth orthoborates, RBO_3 (R = Y, La and Gd), obtained by combustion synthesis. Optical Materials, 27, 1516–1522.

28. Chen, X., Yin, H., Chang, X., Zang, H., Xiao, W., Synthesis, crystalstructure,spectrumproperties,andelectronicstructureof a novelnon - centro symmetric borate, $BiCd_3(AlO)_3(BO_3)_4$. Journal of Solid State Chemistry, 183, 2910–2916, 2010